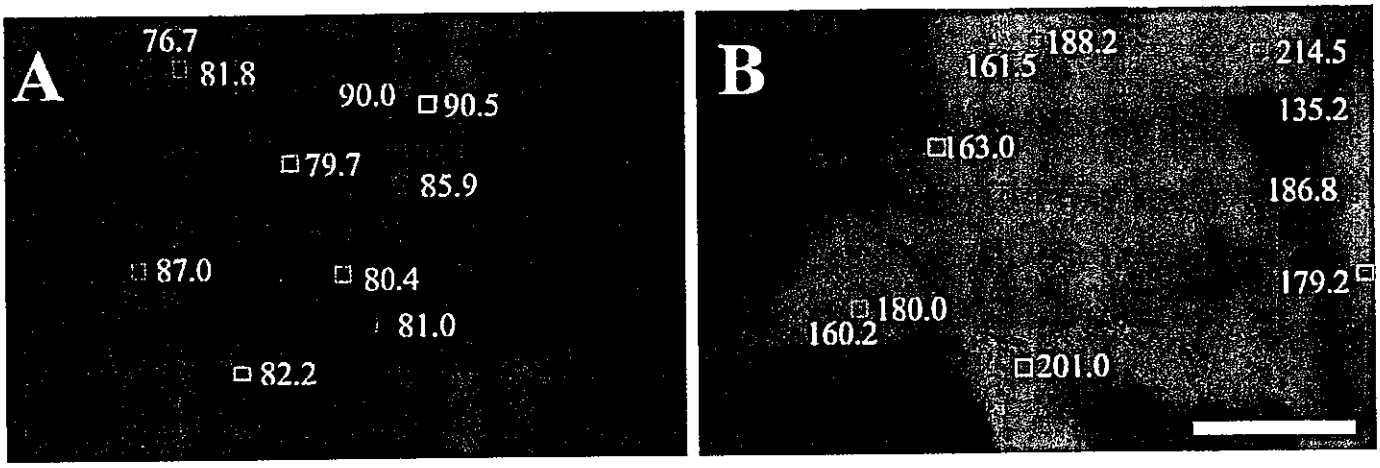

FIG. 2. Immunofluorescence analysis of HO-1 induction in HT22 cells. HT22 cells were treated with vehicle (A) or with 1 μM NEPP11 (B) for 24 h, and then the cells were fixed and stained with anti-(HO-1) antibody. The values in the photographs are average fluorescence intensity (arbitrary units) in the designated squares. Scale bar in B represents 20 μm.

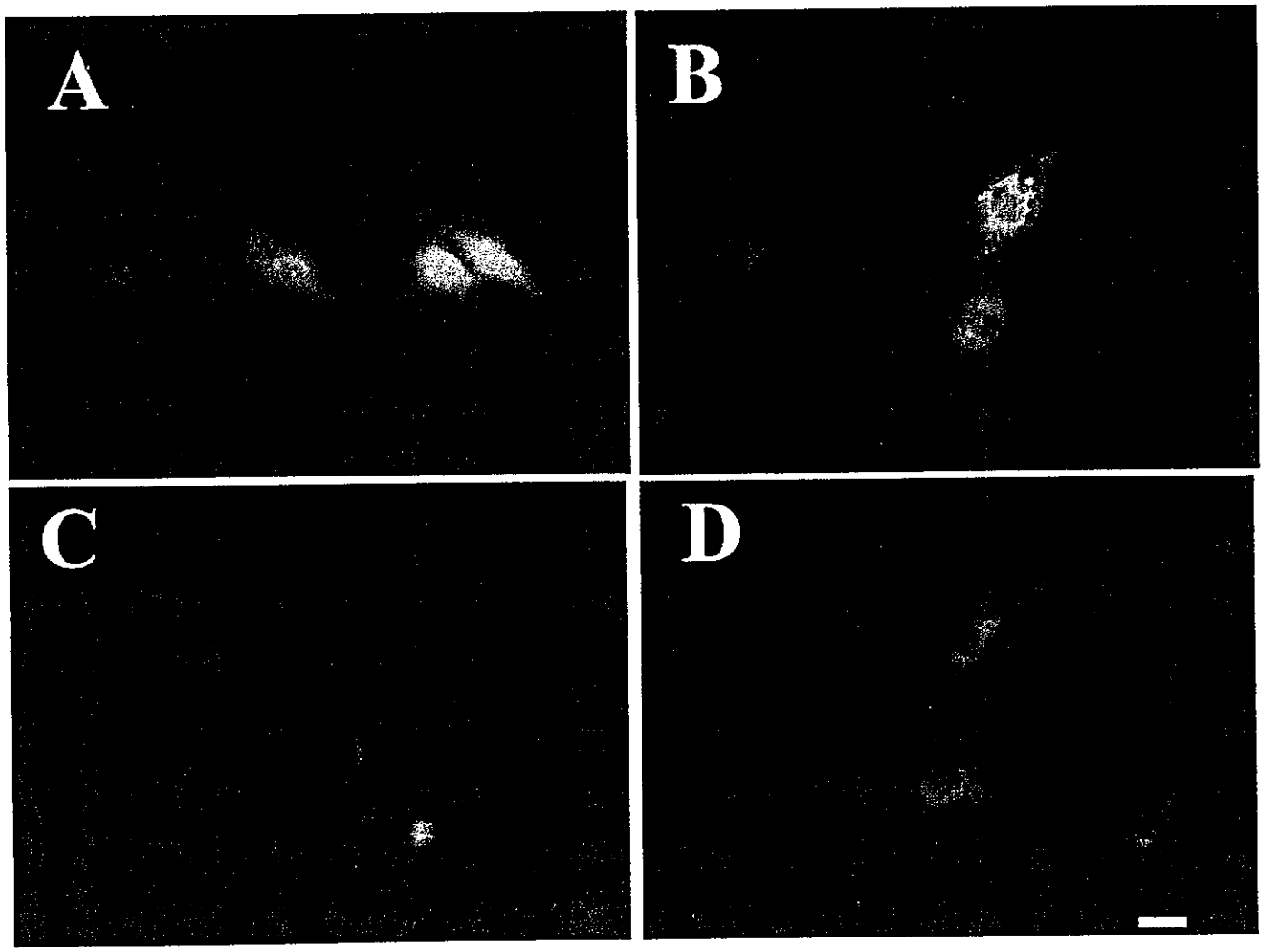

FIG. 3. Protection of HT22 cells against oxidative glutamate toxicity by gene transfer of HO-1. HT22 cell transfected with pEGFPC1 (GFP only, A and C) or pHOC1 (GFP–HO-1, B and D) were incubated for 12 h. Then, glutamate (C and D) or vehicle (A and B) was added; and 24 h later the cells were fixed and observed under a fluorescence microscope. Scale bar in D represents 20 μm.

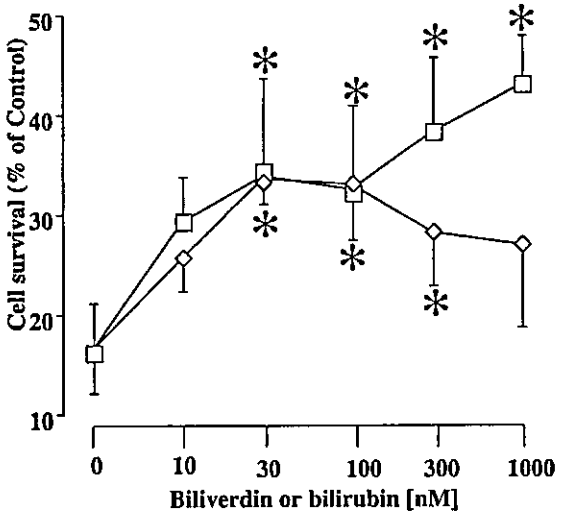

FIG. 4. Effect of biliverdin and bilirubin on the oxidative glutamate toxicity of HT22 cells. HT22 cells were treated with various concentrations of biliverdin or bilirubin in addition to 5 mM glutamate and were then lysed for the MTT assay at 24 h. Open squares, biliverdin; diamonds, bilirubin. The values, which represent the percentage of the control MTT activity, are means + SD ($n = 4$). Significance of the difference in value in the presence of biliverdin or bilirubin vs. the control value (in the absence of these compounds) was determined by ANOVA ($^*P < 0.05$).

catalytic activity was enhanced by phosphorylation and showed that C-kinase, activated by phorbol,12-myristate,13-acetate (PMA), phosphorylated HO-2, resulting in increased activity and that it protects neurons against oxidative stress through enhanced production of biliverdin and bilirubin. In contrast, NEPP11, by inducing HO-1 protein in neurons, caused the cells to produce biliverdin and bilirubin, both of which seem to be responsible for the inhibition of cell death induced by oxidative stress.

We propose an intracellular mechanism for the neuroprotective effect of NEPP11 in Fig. 5. NEPP11 covalently binds to some nuclear protein, and induces HO-1 protein (Narumiya *et al.*, 1987; Parker, 1995; Satoh *et al.*, 2001). The induction of HO-1 is an event responsible for the inhibition of neuronal death by NEPP11 based on the following results. (1) Neuroprotective NEPP6 and NEPP11 induced HO-1 protein in neuronal cells both in the presence and in the absence of glutamate (Fig. 1B); (2) neither non-neuroprotective PG (PGA_2 nor Δ^{12}-PGJ_2) protected the cells or induced HO-1 protein (Fig. 1C); (3) gene transfer of HO-1 protected HT22 cells against oxidative stress (Fig. 3) and (4) biliverdin and bilirubin, products of HO, actively protected HT22 cells against oxidative stress (Fig. 4). NEPP11 binds to cellular protein(s) and activates transcription of HO-1 to protect neurons presumably through enhanced production of biliverdin and bilirubin (Fig. 5). In contrast to a sustained phase of regulation of HO activity derived from HO-1 gene transcription, neurons can also have a transient phase of regulation of HO activity derived from HO-2 protein phosphorylation. Neurons exposed to acute oxidative stress activate HO-2 to resist this stress via phosphorylation of HO-2, whereas those exposed to chronic oxidative stress activate HO-1 through transcription. Regulations of 'heme-pool' by HO-1 and HO-2 have distinct roles in neuronal survival and are highly critical for the resistance to oxidative stress. HO-2 is rapidly activated by phosphorylation, but its activated state is not sustained. In contrast, the HO-1 level is slowly increased by transcription, and is sustained. We consider that these differential regulations of HO activities may co-operatively contribute to the maintenance of neuronal survival under oxidative conditions. Strong therapeutic implications of HO-1 induction in neuronal diseases associated with oxidative stress were provided by the findings that HO-1-deficient mice were strongly susceptible to the deleterious effects of endotoxin or hypoxia (Poss & Tonegawa, 1997; Yet *et al.*, 1999).

Bilirubin, the end-product of heme catabolism in mammals, is generally regarded as a potentially cytotoxic, lipid-soluble waste product that needs to be excreted. However, recent studies suggest that the resultant accumulation of biliverdin and bilirubin might afford a neuroprotective mechanism against oxidative stress. In the present study, bilirubin as well as biliverdin protected HT22 cells at concentrations in the nanomolar range (Fig. 4). Consistent with this finding, Dore *et al.* (1999) also reported that these compounds protected primary cortical neurons against hydrogen peroxide toxicity at similar concentrations. These pharmacological studies suggest that low concentrations (below micromolar levels) of biliverdin and bilirubin might have a neuronal survival effect in the brain, whereas higher concentrations (above micromolar levels) of blirubin were shown to induce neuronal death (Grojean *et al.*, 2000). What is the mechanism of the neuroprotective effects afforded by these endogenous compounds? Several possibilities were postulated by previous investigators. One is the scavenging of free radicals (Stocker *et al.*, 1987), and another is inhibition of protein phosphorylation (Hansen *et al.*, 1997). Because

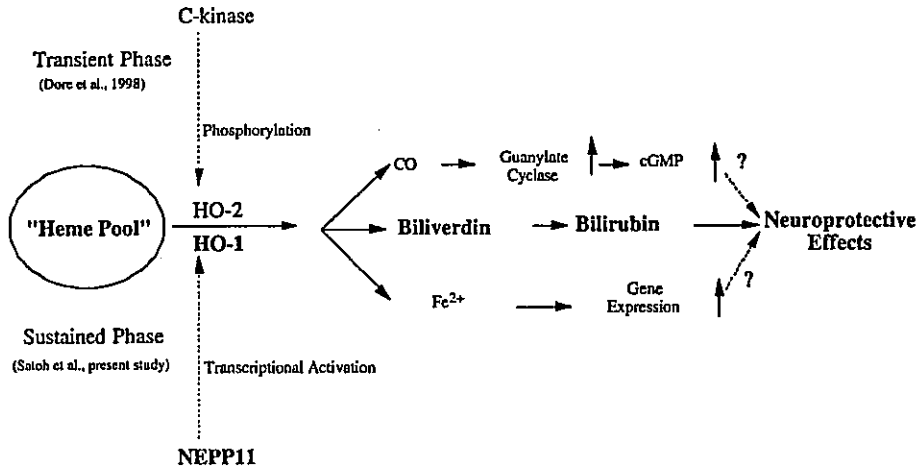

FIG. 5. Proposed mechanism for neuronal survival-promoting effect of NEPP11.

the generation of free radicals (Tan *et al.*, 1998) and protein phosphorylation, for example by ERK1/2 (T. Satoh *et al.*, 2000c; Stanciu *et al.*, 2000), plays a central role in the death of HT22 cells by oxidative glutamate toxicity, inhibition of these events may contribute to inhibition of cell death. The problem is that a high concentration (above micromolar level) of bilirubin is required to produce these actions. Thus, some other unknown mechanism might be responsible for the inhibition of cell death by bilirubin and biliverdin. If not, then several neuroprotective events triggered by induction of HO-1 other than production of biliverdin and bilirubin might be possible. For example, CO is suspected to be a signalling molecule to modulate guanylate cyclase activity and to produce cGMP (Maines, 1997; Zakhary *et al.*, 1997), which reportedly protects primary neurons (Keller *et al.*, 1998).

The biological significance of HO-1 induction has remained a matter of debate. The most essential question is whether HO-1 protects or kills neurons. Schipper (2000) suggested that HO-1 overexpression contributes to pathological iron deposition and mitochondrial damage in ageing-related neurodegenerative disorders. Metalloporphyrins, inhibitors of HO, protected astroglial cells against hydrogen peroxide toxicity (Dwyer *et al.*, 1998). These results suggest that the induction of HO-1 is cytotoxic. However, *in vitro* studies suggest neuroprotective effects of HO-1. Culture experiments to examine the role of HO-1 in neuronal survival were conducted by two groups. One (Le *et al.*, 1999) reported the use of antisense nucleotides; and the other (Chen *et al.*, 2000) reported the use of primary neurons from mice overexpressing HO-1. HO-1 was induced in response to a variety of oxidative stresses including β-amyloid peptides and hydrogen peroxide in neuronal cells; and pretreatment with HO-1 antisense nucleotides enhanced the cytotoxicity, whereas hemin, an HO-1 inducer, decreased the toxicity (Le *et al.*, 1999). Cerebellar granule neurons from mice overexpressing HO-1 resisted glutamate toxicity by decreasing the levels of free radicals (Chen *et al.*, 2000). In addition, CNS neurons of HO-1 transgenic mice were resistant to permanent brain ischaemia (Panahian *et al.*, 1999). These results suggest that HO-1 protein is induced under oxidative conditions and that the HO-1 protein protects neurons against oxidative stress. In view of our results and those of others, it is possible that the enhanced expression of HO-1 in the neurodegenerative areas is not a cause of cell damage but a result of cell defence against oxidative stress.

Natural cyclopentenone PGs (Δ^{12}-PGJ_2 and *15-deoxy*-$\Delta^{12,14}$-PGJ_2) were shown to induce HO-1 protein in non-neuronal cells (Koizumi *et al.*, 1995; Negishi *et al.*, 1995; Clay *et al.*, 2001). Negishi *et al.* (1995) reported that Δ^{12}-PGJ_2 potently induced HO-1 in leukaemia cells through phosphorylation of nuclear protein. The induction of HO-1 protein may contribute to the anti-tumour effects of Δ^{12}-PGJ_2 because adenoviral gene transfer of HO-1 reportedly arrested the cell cycle of, and induced apoptosisin, vascular smooth muscle cells proliferating in response to serum (Liu *et al.*, 2002). In contrast to an apoptosis-inducing effect on proliferating cells, induced HO-1 seems to inhibit cell death in post-mitotic CNS neurons. For example, administration of HO-1 cDNA via viral vectors decreased the volume of infarct induced in the brain by permanent ischaemia, suggesting that HO-1 induction is neuroprotective (Panahian *et al.*, 1999). NEPP11 potently induced HO-1 in cortical neurons (data not shown) as well as HT22 cells and protected them at similar concentrations (Satoh *et al.*, 2001). Furthermore, NEPP11 also reduced the volume of infarct induced by permanent ischaemia (Satoh *et al.*, 2001). In this context, NEPP11 is a novel molecular probe both *in vivo* and *in vitro* for the investigation of neuroprotective HO-1 inducer against oxidative stress. In contrast, non-neuroprotective cyclopentenone PGs such as PGA_1, PGA_2, Δ^{12}-PGJ_2 and *15-deoxy*-$\Delta^{12,14}$-PGJ_2 neither protected HT22 cells (Satoh *et al.*, 2001) nor induced HO-1 protein in them (Fig. 1).

The differential response to Δ^{12}-PGJ_2 between neuronal and non-neuronal cells remains to be analysed, but it might be dependent on the cell types used. Alternatively, the toxicity of Δ^{12}-PGJ_2 toward neurons might mask the neuroprotective effects of this PG.

Acknowledgements

This work was supported in part by the Research for the Future Program (RFTF) JSPS-RFTF 98L00201 of the Japan Society for the Promotion of Science (JSPS) and by Special Coordination Funds for Promoting Science and Technology from the Science and Technology Agency (Japan). We thank Dr Larry D. Frye for editorial help with the manuscript.

Abbreviations

GFP, green fluorescence protein ; HO, heme oxygenase; NEPP11, neurite outgrowth-promoting prostaglandins 11; PG, prostaglandin.

References

Barde, Y.A. (1998) Biological roles of neurotrophins. In Hefti, F. (Ed.), *Neurotrophic Factors*. Springer, Berlin, pp. 1–31.

Bian, J., Wang, Y., Smith, M.R., Kim, H., Jacobs, C., Jackman, J., Kung, H.F., Colburn, N.H. & Sun, Y. (1996) Suppression of in vivo tumor growth and induction of suspension cell death by tissue inhibitor of metalloproteinases (TIMP)-3. *Carcinogenesis*, **17**, 1805–1811.

Chen, K., Gunter, K. & Maines, M.D. (2000) Neurons overexpressing heme oxygenase-1 resist oxidative stress-mediated cell death. *J. Neurochem.*, **75**, 304–313.

Clay, C.E., Atsumi, G., High, K.P. & Chilton, F.H. (2001) Early de novo gene expression is required for *15-deoxy*-$\Delta^{12,14}$-prostaglandin J_2-induced apoptosis in breast cancer cells. *J. Biol. Chem.*, **276**, 47131–47135.

Davis, J.B. & Maher, P. (1994) Protein kinase C activation inhibits glutamate-induced cytotoxicity in a neuronal cell line. *Brain Res.*, **652**, 169–173.

Dore, S., Takahashi, M., Ferris, C.D., Hester, L.D., Guastella, D. & Snyder, S.H. (1999) Birilubin, formed by activation of heme oxygenase-2, protects neurons against oxidative stress injury. *Proc. Natl Acad. Sci. USA*, **96**, 2445–3450.

Dwyer, B.E., Lu, S.Y., Laitinen, J.T. & Nishimura, R.N. (1998) Protective properties of tin- and manganese-centered porphyrins against hydrogen peroxide-mediated injury in rat astroglial cells. *J. Neurochem.*, **71**, 2497–2504.

Ewing, J.F. & Maines, M.D. (1991) Rapid induction of heme oxygenase-1 mRNA and protein by hyperthermia in rat brain: heme oxygenase-2 is not a heat shock protein. *Proc. Natl Acad. Sci. USA*, **88**, 5364–5368.

Fukushima, M. (1992) Biological activities and mechanism of action of PGJ_2 and related compounds: an update. *Prostagl. Leukotri. Essen. Fatty Acids*, **47**, 1–12.

Furuta, K., Tomokiyo, K., Satoh, T., Watanabe, Y. & Suzuki, M. (2000) Designed prostaglandins with neurotrophic activities. *Chembiochem.*, **1**, 283–286.

Gorospe, M., Wang, X., Guyton, K.Z. & Holbrook, N.J. (1996) Protective role of $p21^{Waf1/Cip1}$ against prostaglandin A_2-mediated apoptosis of human colorectal carcinoma cells. *Mol. Cell. Biol.*, **16**, 6654–6660.

Grojean, S., Koziel, V., Vert, P. & Daval, J.L. (2000) Bilirubin induces apoptosis via activation of NMDA receptors in developing rat brain. *Exp. Neurol.*, **166**, 334–341.

Hansen, T.W., Mathiesen, S.B. & Walaas, S.I. (1997) Modulation of the effect of bilirubin on protein phosphorylation by lysine-containing peptides. *Pediatr. Res.*, **42**, 615–617.

Holbrook, N.J., Carlson, S.G., Choi, A.M.K. & Fargnoli, J. (1992) Induction of HSP70 gene expression by antiproliferative prostaglandin PGA_2: a growth-dependent response mediated by activation of heat shock transcription factor. *Mol. Cell. Biol.*, **12**, 1528–1538.

Honn, K.V., Bockman, R.S. & Marnett, L.J. (1981) Prostaglandins and cancer: a review of tumor initiation through tumor metastasis. *Prostaglandins*, **21**, 833–864.

Ishii, M., Hashimoto, S., Tsutsumi, S., Wada, Y., Matsushima, K., Kodama, T. & Aburatani, H. (2000) Direct comparison of Genechip and SAGE on the quantitative accuracy in transcript profiling analysis. *Genomics*, **68**, 136–143.

Ishikawa, T., Akimaru, K., Nakanishi, M., Tomokiyo, K., Furuta, K., Suzuki, M. & Noyori, R. (1998) Anticancer prostaglandin-induced cell cycle arrest and its modulation by GS-X pump inhibitor. *Biochem. J.*, **336**, 569–576.

Keller, J.N., Hanni, K.B., Mattson, M.P. & Markesbery, W.R. (1998) Cyclic nucleotides attenuate lipid peroxidation-mediated neuron toxicity. *Neuroreport*, **16**, 3731–3734.

Koizumi, T., Odani, N., Okuyama, T., Ichikawa, A. & Negishi, M. (1995) Identification of a cis-regulatory element for delta 12-prostaglandin J_1-induced expression of the rat heme oxygenase gene. *J. Biol. Chem.*, **270**, 21779–21784.

Kubo, T., Nonomura, T., Enokido, Y. & Hatanaka, H. (1995) Brain-derived neurotrophic factor (BDNF) can prevent apoptosis of rat cerebellar granule neurons in culture. *Dev. Brain Res.*, **85**, 249–258.

Le, W., Xie, W. & Appel, S.H. (1999) Protective role of heme oxygenase-1 in oxidative stress-induced neuronal injury. *J. Neurosci. Res.*, **56**, 652–658.

Liu, X.M., Chapman, G.B., Wang, H. & Durante, W. (2002) Adenovirus-mediated heme oxygenase-1 gene expression stimulates apoptosis in vascular smooth muscle cells. *Circulation*, **105**, 79–84.

Maines, M.D. (1997) The heme oxygenase system: a regulation of second messenger gases. *Annu. Rev. Pharmacol. Toxicol.*, **37**, 517–554.

McAllister, A.K. (2000) Biolistic transfection of neurons. Sci. STKE PL1.

McMahon, S.B. & Priestly, J.V. (1995) Peripheral neuropathies and neurotrophic factors: animal model and clinical perspectives. *Curr. Opin. Neurbiol.*, **5**, 614–616.

Mehlen, P., Kretz-Remy, C., Preville, X. & Arrigo, A.P. (1996) Human hsp27, *Drosophila* hsp27 and human alphaB-crystallin expression-mediated increase in glutathione is essential for the protective activity of these proteins against TNFalpha-induced cell death. *EMBO J.*, **15**, 2695–2706.

Mosmann, T. (1983) Rapid colorimetric assay for cellular growth and survival: application to proliferation and cytotoxic assay. *J. Immunol. Methods*, **65**, 55–63.

Narumiya, S., Ohno, K., Fukushima, M. & Fujiwara, M. (1987) Site and mechanism of growth inhibition by prostaglandins. III. Distribution and binding of prostaglandin A_2 and Δ^{12}-prostaglandin J_2 in nuclei. *J. Pharmacol. Exp. Therap.*, **242**, 306–311.

Negishi, M., Odani, N., Koizumi, T., Takahashi, S. & Ichikawa, A. (1995) Involvement of protein kinase in delta12-prostaglandin J2-induced expression of rat heme oxygenase-1 gene. *FEBS Lett.*, **372**, 279–282.

Panahian, N., Yoshihara, M. & Maines, M.D. (1999) Overexpression of heme oxygenase-1 is neuroprotective in a model of permanent middle cerebral artery occlusion in transgenic mice. *J. Neurochem.*, **72**, 1187–1203.

Parker, J. (1995) Prostaglandin A_2 protein interactions and inhibition of cellular proliferation. *Prostaglandins*, **50**, 359–375.

Poss, K.D. & Tonegawa, S. (1997) Reduced stress defense in heme oxygenase 1-deficient cells. *Proc. Natl Acad. Sci. USA*, **94**, 10925–10930.

Saragovi, H.U. & Gehring, K. (2000) Development of pharmacological agents for targeting neurotrophins and their receptors. *Trends Phamarcol. Sci.*, **21**, 93–98.

Satoh, H., Matsuda, H., Kawamura, T., Isogai, M., Yoshikawa, N. & Takahashi, T. (2000) Intracellular distribution, cell-to-cell trafficking and tubule-inducing activity of the 50 kDa movement protein of *Apple chlorotic leaf spot virus* fused to green fluorescent protein. *J. Gen. Virol.*, **81**, 2085–2093.

Satoh, T., Furuta, K., Suzuki, M. & Watanabe, Y. (2002) Neurite outgrowth-promoting prostaglandins that act as neuroprotective agents against brain ischemia and may enhance recovery of higher neuronal functions. In Kikuchi, H. (Ed.), *Strategenic Medical Science Against Brain Attack*. Springer-Verlag, Tokyo, pp. 78–93.

Satoh, T., Furuta, K., Tomokiyo, K., Nakatsuka, D., Miura, M., Hatanaka, H., Ikuta, K., Suzuki, M. & Watanabe, Y. (2000a) Facilitatory roles of novel compounds designed from cyclopentenone prostaglandins on the neurite outgrowth-promoting activities of NGF. *J. Neurochem.*, **75**, 1092–1102.

Satoh, T., Furuta, K., Tomokiyo, K., Namura, S., Nakatsuka, D., Sugie, Y., Ishikawa, Y., Hatanaka, H., Suzuki, M. & Watanabe, Y. (2001) Neurotrophic actions of novel compounds designed from cyclopentenone prostaglandins. *J. Neurochem.*, **77**, 50–62.

Satoh, T., Furuta, K., Tomokiyo, K., Suzuki, M. & Watanabe, Y. (2000b) Designed cyclopentenone prostaglandin derivatives as neurite outgrowth-promoting compounds for CAD cells, a rat catecholaminergic neuronal cell line of the central nervous system. *Neurosci. Lett.*, **291**, 167–170.

Satoh, T., Nakatauka, D., Watanbabe, Y., Nagata, N., Kikichi, H. & Namura, S. (2000c) Neuroprotection by MEK/ERK kinase inhibition against oxidative stress in a mouse neuronal cell line and rat primary cultured neurons. *Neurosci. Lett.*, **288**, 163–166.

Schipper, H.M. (2000) Heme oxygenase-1: role in brain aging and neurodegeneration. *Exp. Gerentol.*, **35**, 821–830.

Schubert, D., Kimura, H. & Maher, P. (1992) Growth factors and vitamin E modify neuronal glutamate toxicity. *Proc. Natl Acad. Sci. USA*, **89**, 8264–8267.

Shibahara, S. (1994) Heme oxygenase-regulation and physiological implication in heme metabolism. In Fujita, H. (Ed.), *Regulation of Heme Protein Synthesis*. AlphaMed. Press, Dyton, pp. 103–116.

Shibahara, S., Muller, R., Taguchi, H. & Yoshida, T. (1985) Cloning and expression of cDNA for rat heme oxygenase. *Proc. Natl Acad. Sci. USA*, **82**, 7865–7869.

Stanciu, M., Wang, Y., Kentor, R., Burke, N., Watkins, S., Kress, G., Reynolds, I., Klann, E., Angiolieri, M.R., Johnson, J.W. & DeFranco, D.B. (2000) Persistent activation of ERK contributes to glutamate-induced oxidative toxicity in a neuronal cell line and primary cortical neuron cultures. *J. Biol. Chem.*, **275**, 12200–12206.

Stocker, R., Yamamoto, Y., McDonagh, A.F., Glazer, A.N. & Ames, B.N. (1987) Bilirubin is an antioxidant of possible physiological importance. *Science*, **235**, 1043–10436.

Suzuki, M., Kiho, T., Tomokiyo, K., Furuta, K., Fukushima, S., Takeuchi, Y., Nakanishi, M. & Noyori, R. (1998) Rational design of antitumor prostaglandins with high biological stability. *J. Med. Chem.*, **41**, 3084–3090.

Suzuki, M., Mori, M., Niwa, T., Hirata, R., Ishikawa, T. & Noyori, R. (1997) Chemical implication for antitumor antiviral prostaglandins: reaction of Δ^7-prostaglaindin A_1 and prostaglandin A_1 methyl esters with thiol. *J. Am. Chem. Soc.*, **119**, 2376–2385.

Tanikawa, M., Yamada, K., Tominaga, K., Morisaki, H., Kaneko, Y., Ikeda, K., Suzuki, M., Kiho, T., Tomokiyo, K., Furuta, K., Noyori, R. & Nakanishi, M. (1998) Potent prostaglandin A_1 analogs that suppress tumor cell growth through induction of p21 and reduction of cyclin E. *J. Biol. Chem.*, **273**, 18522–18527.

Yet, S.F., Perrella, M.A., Layne, M.D., Hsieh, C.M., Maemura, K., Kobik, L., Wiesel, P., Christou, H., Kourembanas, S. & Lee, W.S. (1999) Hypoxia induces severe right ventricular dilatation and infarction in heme oxygenase-1 null mice. *J. Clin. Invest.*, **103**, R23–R29.

Zakhary, R., Poss, K.D., Jaffrey, S.R., Ferris, C.D., Tonegawa, S. & Snyder, S.H. (1997) Targeted gene deletion of heme oxygenase 2 reveals neuronal role for carbon monoxide. *Proc. Natl Acad. Sci. USA*, **94**, 14848–14853.

[CANCER RESEARCH 63, 8629–8633, December 15, 2003]

An Opposing View on WWOX Protein Function as a Tumor Suppressor

Akira Watanabe,[1] Yoshitaka Hippo,[1] Hirokazu Taniguchi,[1] Hiroko Iwanari,[3] Masakazu Yashiro,[4] Kosei Hirakawa,[4] Tatsuhiko Kodama,[2] and Hiroyuki Aburatani[1]

[1]Genome Science Division and [2]Laboratory of Systems Biology and Medicine, Research Center for Advanced Science and Technology, The University of Tokyo, Tokyo; [3]Perseus Proteomics, Inc., Tokyo; and [4]First Department of Surgery, Osaka City University Medical School, Osaka, Japan

ABSTRACT

WW domain-containing oxidoreductase (*WWOX*) is a candidate tumor suppressor gene. Because mutation or deletion in the coding region of *WWOX* is rarely found, it is speculated that the appearance of aberrant transcripts affects progression of various cancers. However, little is known about the role in these cancers of the WWOX protein. To characterize endogenous WWOX proteins, we analyzed WWOX expression using newly generated monoclonal antibodies. In immunoblot analysis of 49 cancer cell lines, only the normal form of the protein was detectable, although some of cell lines exhibited aberrant *WWOX* RNA transcripts. Accumulation of truncated proteins was observed by inhibiting proteasomal degradation with MG-132, whereas expression level of normal protein did not change, suggesting truncated proteins may be subjected to rapid degradation through proteasomal machinery. Immunohistochemistry for cancer cells demonstrated that WWOX protein levels are not decreased but rather elevated in gastric and breast carcinoma, challenging the notion of WWOX as a classical tumor suppressor. In noncancerous cells, WWOX was observed only in epithelial cells, including hormone-regulated cells such as Leydig cells, follicular cells, prostate epithelium, and mammary glands. Interestingly, restricted staining in nuclei was observed in some mammary gland cells while other epithelial cells exhibited localization of WWOX in cytoplasm. Nuclear localization of WWOX was also confirmed in confluent human fibroblast KMS-6, whereas WWOX was associated mainly with mitochondria before reaching confluence, indicating that WWOX shuttles between cytoplasm and nuclei. These findings provide novel insights into aspects of human WWOX function in both normal and malignant cells.

INTRODUCTION

Common fragile sites can contribute to oncogenesis by facilitating gene inactivation through chromosomal deletion or amplification (1). The common fragile site *FRA16D* on chromosome 16q23.3-24.2 is localized within a large region of chromosomal instability in cancers defined by loss of heterozygosity (2–5) and homozygous deletion (6, 7). Mashimo *et al.* (8) reported that microcell-mediated chromosome transfer of chromosome 16q23-24 resulted in strong suppression of metastatic activity in prostatic cancer cell lines, indicating the presence of a major tumor suppressor gene associated with cancer progression on 16q23.3-24.2.

WW domain-containing oxidoreductase (*WWOX*) was cloned from this *FRA16D* site (9, 10). From its deduced amino acid sequence, two functional domains were predicted; the first, at the NH_2 terminus, is a tandem WW domain that is likely to be involved in protein-protein interactions. The second is short-chain dehydrogenase/reductase domain that is shared in common among metabolic enzymes of steroid hormones (11). On the basis of the function of these motifs and the observation that *WWOX* shows elevated expression in hormonally regulated tissues such as testis, prostate, and ovary, it has been speculated that WWOX is functionally related to steroid hormones (9).

WWOX is reported to behave aberrantly in cancers of the breast, ovary, esophagus, and lung (9, 12–16). Although truncated *WWOX* transcripts are frequently observed in cancers from these tissues, mutations or deletions of the gene in the coding region are rarely found. Ectopic expression of WWOX protein induces apoptosis (11) and suppression of tumor growth both *in vitro* and *in vivo* (17). From these findings, *WWOX* was proposed to be a candidate tumor suppressor gene in which the function is presumably inactivated by the dominant negative action of truncated products from aberrant transcripts (17). However, a consistent picture of the subcellular localization of WWOX has not yet emerged (11, 17), and the dominant negative theory of WWOX action has remained untested without direct examination of endogenous expression of WWOX protein. Consequently, little is known about the role of WWOX protein in cancer progression.

To address these issues, we performed immunoblotting, subcellular localization analysis, and immunohistochemistry using newly generated monoclonal antibodies and provide new insights into the molecular understanding of WWOX protein in normal and cancer cells.

MATERIALS AND METHODS

Tumor Cell Lines. The stomach cancer cell lines OCUM-2M, OCUM-2MD3, and OCUM-2MLN were previously established by Yashiro *et al.* (18) and Fujiwara *et al.* (19). An additional 46 tumor cell lines derived from different tumor types (stomach, liver, lung, colon, esophagus, pancreas, kidney, brain, and breast) were obtained from the American Type Culture Collection (Manassas, VA), Riken Cell Bank (Tsukuba, Japan), Cell Resource Center for Biomedical Research at Tohoku University (Sendai, Japan), and Japanese Collection of Research Bioresources (Tokyo, Japan). Human skin fibroblast KMS-6 was purchased from Dainippon Pharmaceutical Co. Ltd. (Osaka, Japan)

Reverse Transcription-PCR and Northern Blot Analysis. cDNA derived from human *WWOX* was synthesized with oligodeoxythymidylic acid primer from 1 μg of total RNA and diluted up to 80 μl as described previously (20). Reverse transcription-PCR was performed with Advantage cDNA polymerase mixture (Clontech, Palo Alto, CA) and 1 μl of cDNA for 1 cycle of 94°C for 2 min, followed by 35 cycles of 94°C for 30 s, 63°C for 30 s, and 68°C for 3 min. Primers for amplification of sequence from exon 1 to 9 were 5′-GTGCCTCCACAGTCAGCCATG-3′ (sense) and 5′-CATCCCTCCCAGACCCTCCAGT-3′ (antisense). Glyceraldehyde-3-phosphate dehydrogenase primers were CATGTGGGCCATGAGGTCCACCAC (sense) and AATGCCTCCTGCACCACCAACTGC (antisense). Northern blot analysis and quantification of mRNA expression, using 20 μg of total RNA encoding normal *WWOX*, was performed as described previously (20).

Generation of Anti-WWOX Monoclonal Antibodies. A glutathione *S*-transferase-fusion protein of human WWOX derived from normal tissue was constructed in the expression vector pET 41 (Novagen, Madison, WI). Fusion proteins were induced in BL-21 Codon Plus (DE3; Stratagene, La Jolla, CA)

Received 4/18/03; revised 9/16/03; accepted 9/29/03.

Grant support: Grants-in-Aid for Scientific Research (B) 12557051 and 13218019 and Scientific Research on Priority Areas (C) 12217031 from Ministry of Education, Culture, Sports, Science and Technology (H. A.). This study was carried out as a part of The Technology Development for Analysis of Protein Expression and Interaction in Bioconsortia on R&D of New Industrial Science and Technology Frontiers which was supported by Industrial Science, Technology and Environmental, Policy Bureau, Ministry of Economy, Trade and Industry and delegated to New Energy Development Organization.

The costs of publication of this article were defrayed in part by the payment of page charges. This article must therefore be hereby marked *advertisement* in accordance with 18 U.S.C. Section 1734 solely to indicate this fact.

Note: Drs. Watanabe and Hippo contributed equally to this study.

Requests for reprints: Hiroyuki Aburatani, Genome Science Division, Research Center for Advanced Science and Technology, The University of Tokyo, 4-6-1, Komaba, Meguro-ku, Tokyo 153-8904, Japan. Phone: 81-3-5452-5352; Fax: 81-3-5452-5355; E-mail: haburata-tky@umin.ac.jp.

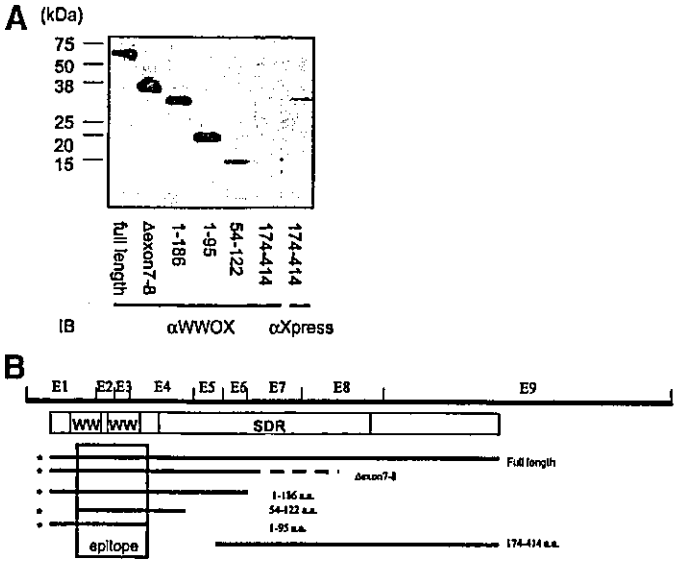

Fig. 1. Epitope mapping of anti-WWOX monoclonal antibody H2267. *A*, immunoblot analysis was performed with anti-WWOX antibody H2267 (*Lanes 1–6*) and anti-Xpress antibody (*Lane 7*). Xpress-tagged proteins were obtained by transfection of expression vector with inserts into COS7 cells. *B*, a schematic representation of various recombinant WWOX proteins, *asterisk marked bars* indicate the deduced region where the epitope of antibody H2267 resides.

and purified using Glutathione Sepharose 4B (Amersham Biosciences, Uppsala, Sweden) according to the manufacture's instructions. Recombinant glutathione *S*-transferase-WWOX was used for 3 cycles of immunization against female BALB/c mice. Spleen cells were isolated and fused with NS-1 myeloma cells (Dainippon Pharmaceutical Co., Ltd.). Hybridomas were selected by ELISA against the purified recombinant glutathione *S*-transferase-fused WWOX. After ELISA against glutathione *S*-transferase-WWOX, 90 hybridoma clones were selected and purified by limited dilution. For mass production, 7 clones of hybridomas were grown in mice ascites. Ascite fluids were collected and purified using ammonium sulfate.

Epitope Mapping. To obtain an antibody that recognizes both normal full-length and truncated proteins, we determined the epitope of each antibody by immunoblotting with recombinant normal and truncated WWOX proteins to correspond to amino acids 1–186, 1–98, amino acids 54–122, amino acids 171–414, and Δexon7–8 inserted into expression vector pcDNA4/HisMax (Invitrogen, Carlsbad, CA). Expression vectors with inserts were transfected into COS-7 using FuGENE 6 Transfection Reagent (Roche, Mannheim, Germany). Recombinant WWOX proteins containing the NH_2-terminal leader peptide Xpress epitope were obtained 2 days after transfection, and expression of proteins were confirmed by immunoblotting with anti-Xpress antibody (Invitrogen) and antimouse IgG antibody according to the following procedure.

Immunoblot Analysis. Proteins (10 μg) were resolved on 12% SDS-PAGE and transferred to polyvinylidene difluoride membranes (Hybond-P; Amersham Biosciences, Piscataway, NJ). After blocking the membranes with 2% nonfat milk in PBS for 1 h, immunoblotting was performed with an anti-WWOX antibody H2267 as primary antibody. Peroxidase-conjugated antimouse IgG antibody (Amersham Biosciences) was used as secondary antibody, and ECL-PLUS Detection System (Amersham Biosciences) was used as substrate for chemiluminescent detection. Quantification of WWOX protein level was performed on a Densitograph Lane and Spot Analyzer (Atto, Tokyo, Japan). To examine rapid degradation of truncated proteins, an inhibition of proteasomal machinery assay was performed using the proteasome inhibitor MG-132, obtained from the Peptide Institute (Osaka, Japan). A total of 5 μM MG-132 dissolved in DMSO or DMSO only was used to treat HCT-116 cells for 10 h, followed by immunoblot analysis.

Immunohistochemical Analysis. Immunohistochemical analysis was performed against samples from a formalin-fixed, paraffin embedded tissue archive. Tissue collection and the subsequent study had full local research ethics approval. The sections were deparaffinised in xylene, washed in ethanol, and rehydrated in Tris-buffered saline. Antigen retrieval was performed in 10 mM citrate buffer pH 7.0 at 120°C for 10 min, followed by incubation with 2% nonfat milk in Tris-buffered saline. Sections were then incubated an antibody H2267 (50 μg/ml) for 1 h, followed by secondary staining with Dako Envision+ (Dako Ltd., Cambridge, United Kingdom). All sections were counter stained with Mayer's hematoxylin.

Subcellular Localization Analysis. Immunostaining of culture cells were performed after fixation in 4% paraformaldehyde and permeabilization in 0.2% Triton X-100 followed by incubation with 2% nonfat milk in Tris-buffered saline. To gain higher, an antibody in immunostaining were biotinylated by reacting antibodies with *N*-hydroxysuccinimide biotin. A biotinylated antibody H2267-biotin (50 μg/ml) was applied as primary antibody for 1 h and FITC-labeled Avidin (Vector Laboratories, Inc., Burlingame, CA) was used as secondary reagent. Dual-color detection by confocal laser scan microscopy was performed after treatment with a 0.5 μM solution of the mitochondrial stain MitoTracker Red CMXRos (Molecular Probes, Inc., Eugene, OR).

RESULTS

Generation and Characterization of Monoclonal Antibodies against Human WWOX. We established 90 clones of hybridoma producing antihuman WWOX antibodies. To select antibodies that can recognize both normal and truncated proteins, we performed epitope mapping for antibodies from 7 clones. Antibody H2267 recognized a region within amino acids 54–98 (Fig. 1*A*). All truncated WWOX proteins with Δexon 5–8, Δexon 6–8 and a novel isoform Δexon7–8, described below in this study, possess amino acids 1–136. Thus, antibody H2267 can recognize both normal and truncated WWOX proteins and was selected for use in the following study.

Expression Analysis of WWOX Transcripts and Proteins in Cancer Cell Lines. We examined the expression of *WWOX* by reverse transcription-PCR in 49 cancer cell lines derived from stomach, liver, lung, colon, esophagus, pancreas, kidney, brain, and breast. Except for the gastric cancer cell line MKN7 that lacks full-length transcripts containing exons 1–9, all of the 48 remaining cell lines expressed full-length transcripts containing exons 1–9. In addition to full-length transcripts, aberrant transcripts were found in OCUM-2MD3, SCH, AGS, LoVo, HCT-116, Capan-1, and MCF-7 (Fig. 2*A*). Sequence analysis of these transcripts revealed a novel aberrant transcript in OCUM-2MD3 and HLE in which alternative splicing resulted in the absence of exons 7–8.

Next, we examined the expression of WWOX proteins in cancer cells by immunoblot analysis. We anticipated the presence of truncated proteins corresponding to the aberrant transcripts identified in

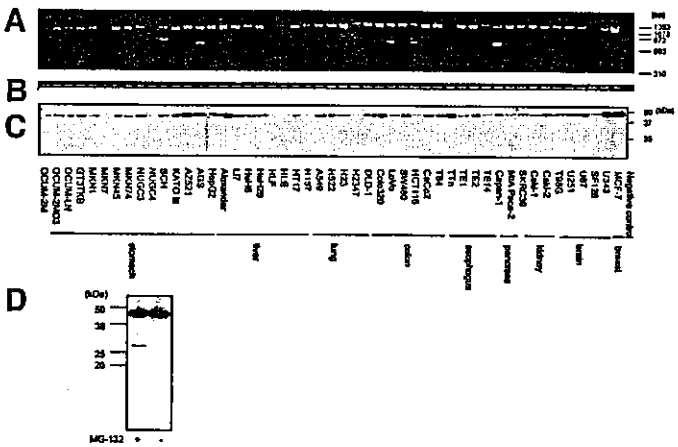

Fig. 2. Expression of *WWOX* transcripts and proteins in cancer cell lines. *A*, reverse transcription-PCR for amplification of fragments containing exons 1–9 of *WWOX*. *B*, reverse transcription-PCR for *GAPDH* as an internal control. *C*, immunoblot analysis of WWOX using anti-WWOX antibody H2267. Note only normal WWOX protein was detected. *D*, proteasome inhibitor MG-132 (5 μM) induced accumulation of truncated protein of WWOX in HCT-116 cells. + and − indicates with or without MG-132, respectively.

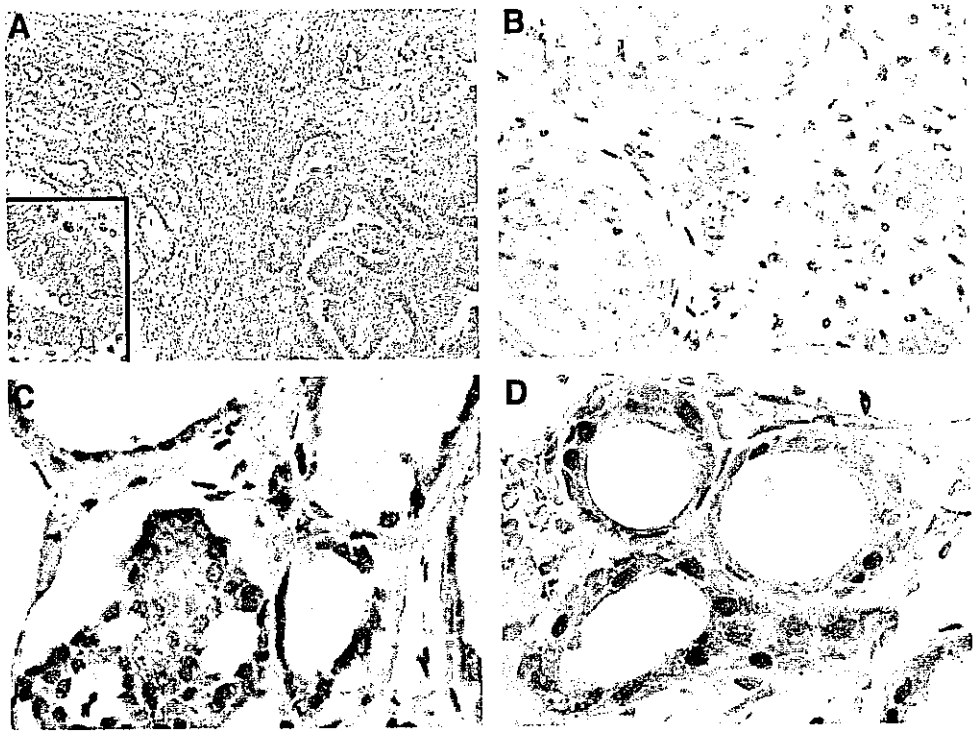

Fig. 3. Immunohistochemical analysis of WWOX. *A*, strong staining is observed in gastric cancer cell (*right* and *inset*), but only weak staining in normal epithelium (*top left*) and no staining in intestinal metaplasia (*bottom left*) was observed in gastric cancer tissue (×100). Magnification is shown in *inset* (×400). *B*, strong staining in Leydig cells (*center*) and weak staining in testicular epithelium is observed in testis (×200). *C*, strong staining in follicular epithelium was observed in thyroid (×400). *D*, restricted nuclear staining is observed in some cells, whereas most cells showed reactivity in cytoplasm in mammary glands (×400).

seven of the cell lines. However, truncated proteins of M_r 35,000 for Δexon5–8, M_r 26,100 for Δexon 6–8, and M_r 35,200 for Δexon7–8, that would correspond to the truncated *WWOX* mRNA transcripts could not be identified in any of the seven cell lines. The 48 cell lines, except for MKN7, expressed a normal WWOX protein (Fig. 2*C*).

Mechanism for Truncated WWOX Protein Absence. We next investigated the reason why truncated products from aberrant transcripts were not detected by immunoblotting. We first suspected that the small amount of aberrant transcripts in cell lines was undetectable: Even in cells with a relatively large amount of aberrant transcripts such as Capan-1 and MCF7, the quantitative ratio of aberrant to normal transcripts determined by Northern blotting was 0.63 and 0.069, respectively. However, truncated proteins could readily be detected in HCT-116 cells treated with the proteasome inhibitor MG-132 (Fig. 2*D*), whereas expression levels of normal WWOX remained unchanged, suggesting that truncated WWOX proteins are not usually detectable due to rapid and selective degradation.

Immunohistochemistry in Tumor and Normal Tissues. To describe WWOX expression *in vivo*, immunohistochemical analysis was performed. If WWOX is a tumor suppressor, decreased expression may be expected in cancer. However, strong staining in cytoplasm was unexpectedly observed in 10 of 16 cases of gastric carcinoma (Fig. 3*A*) and 5 of 5 cases of breast carcinoma (data not shown), whereas staining in surrounding noncancerous cells was weak. In normal tissues, staining was observed only in epithelial cells, particularly in hormone-regulated organs such as testis (Fig. 3*B*), thyroid (Fig. 3*C*), prostate, and mammary glands, consistent with the previous analysis by Northern blotting (9) and our Gene Expression Database by oligonucleotide microarray.[5] In testis, WWOX was enriched in Leydig cells, which are known to produce testosterones (Fig. 3*B*). Interestingly, staining in nucleus was observed in mammary epithelia (Fig. 3*D*), whereas other epithelial cells were stained in the cytoplasm (Fig. 3, *A–C*).

Subcellular Localization Analysis in Culture Cells. Subcellular localization of endogenous WWOX in cultured cells was determined by confocal laser scan microscopy analysis. Dual-color detection of WWOX and mitochondria demonstrated that localization of WWOX was mainly to mitochondria (Fig. 4, *A–C*). However, as shown in Fig. 4*D*, WWOX translocates into nuclei under confluent culture conditions.

DISCUSSION

The present study is an extension of our initial goal of identifying tumor suppressor loci in gastric cancer. We had searched for genomic homozygous deletions in the highly metastatic schirrous gastric cancer cell line OCUM-2MD3 using representational differential analysis with isogenic gastric fibroblast as a reference. This analysis identified several homozygously deleted fragments of ~300bp, including fragments mapped in 3p14 and 16q23, latterly identified as intronic region of *fragile histidine triad* at *FRA3B* and *WWOX* at *FRA16D*, respectively. Both fragments were deleted during malignant progression to OCUM-2MD3 from OCUM-2M, a poorly metastatic and isogenic ancestral line of OCUM-2MD3. As well as *fragile histidine triad*, alterations in *WWOX* such as rare point mutations and frequent intronic deletions and expression of aberrant transcripts found in gastric cancers (unpublished results). Prompted by these notable similarities of *WWOX* to *fragile histidine triad*, which now established as a tumor suppressor after a long period of controversy (21), we set out to analyze WWOX at the protein level.

To make sure of WWOX as a tumor suppressor, the following two points are needed: (*a*) whether protein expression of WWOX in cancer declines; and (*b*) what impact of aberrant transcripts in cancer has (17). To verify these issues, we focused on chasing a fate of aberrant transcripts and making protein expression in cancer clear by immunohistochemistry.

By immunoblotting with an antibody, which can recognize both full-length and truncated WWOX, we were not able to detect truncated proteins and only detected normal WWOX proteins from cell lines, which expressed normal and truncated RNA transcripts. Truncated proteins were not detectable under physiological condition until proteasomal inhibitor MG-132 was treated(Fig. 2*D*). These observa-

[5] http://www2.genome.rcast.u-tokyo.ac.jp/database/.

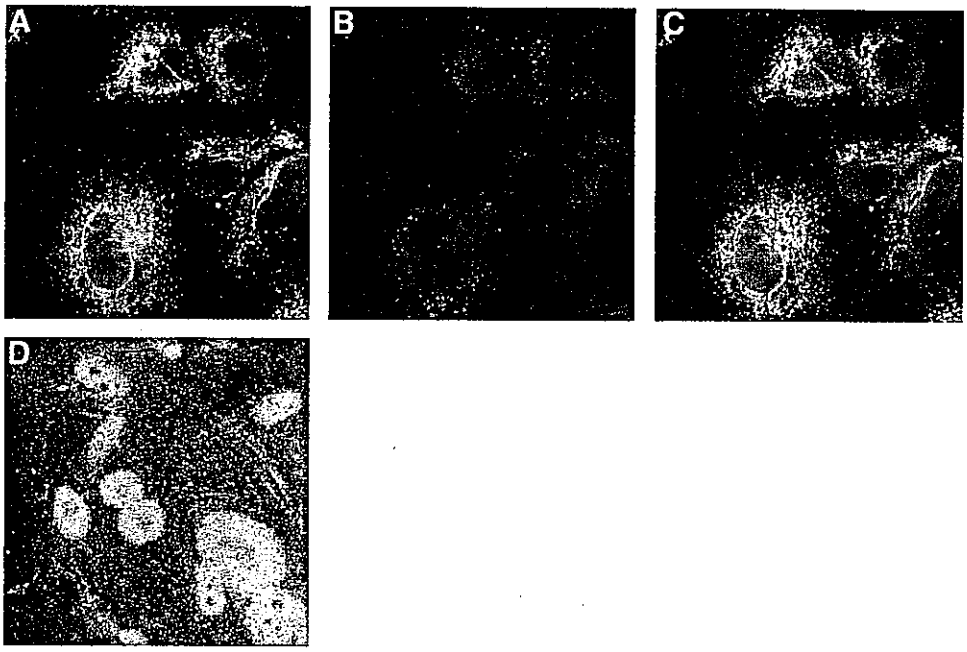

Fig. 4. Subcellular localization of WWOX in human skin fibroblast KMS-6 cells by laser confocal microscopy. *A*, WWOX protein stained with anti-WWOX antibody A2267. *B*, mitochondria stained with MitoTracker Red CMXRos. *C*, merged image demonstrates localization of endogenous WWOX protein in mitochondria. *D*, WWOX translocates into nucleus in KMS-6 under confluent culture conditions.

tions indicate that truncated WWOX proteins in cancer are unstable and subject to rapid proteasomal degradation and contradicts the possibility that truncated WWOX proteins acts in a dominant negative manner. On account of the possibility that mutated WWOX acts in the dominant negative manner, we examined sequence analysis in the coding region. Cancer-specific missense mutations in coding region were not found in 49 cell lines examined, although polymorphism, which were identified in normal individuals, were found in these cell lines (data not shown). This result is consistent to a report by Paige *et al.* (12), indicating that cancer progression is rarely caused by mutation of WWOX.

Our immunohistochemical analysis in most specimens examined showed expression of WWOX in cancer cells is rather elevated by comparison with that in noncancerous cells. Therefore, we did not find predicted evidences of WWOX as a tumor suppressor. Aberrant transcripts of *WWOX* could be produced as a result of chromosomal instability in 16q23.3-24.2 region, where another tumor suppressor gene might reside. Thus, at present, we cannot conclude that WWOX is a tumor suppressor.

We next examined localization of WWOX protein. A consistent picture of the subcellular localization of WWOX has yet to emerge: localization of ectopic WWOX in Golgi apparatus was observed by Bednarek *et al.* (17), whereas Chang *et al.* (11) reported that endogenous WWOX is localized in mitochondria and translocated to nuclei after tumor necrosis factor α stimulation. The discrepancy between two previous studies in the subcellular localization of WWOX may be caused by the difference between endogenous and ectopic expression. We confirmed that intrinsic WWOX localizes mainly in mitochondria and translocates into nuclei under confluent culture conditions. Because nuclear localization of WWOX was also detected *in vivo*, this translocation may be relevant to its function. Our observations are consistent with the report by Chang *et al.*, who demonstrated interaction of WWOX with p53 (11) and phosphorylation of Tyr^{33} within WW domain by c-Jun NH_2-terminal kinase 1 (22). Shifting of WWOX localization may be controlled by phosphorylation of tyrosine within the WW domain.

In summary, to our knowledge, this is the first article describing expression of WWOX protein in cancers. Our results show there is little possibility that aberrant transcripts in cancer cells behave in a dominant negative fashion. Besides, immunohistochemical analysis in this study was not able to detect down-regulation of WWOX protein in cancer. Thus, our result by protein expression analysis using specific antibody did not support WWOX as a tumor suppressor. Additional characterization of WWOX protein such as mechanism of WWOX translocation will be required to elucidate its function.

ACKNOWLEDGMENTS

We gratefully acknowledge Drs. Shuichi Tsutsumi, Shumpei Ishikawa, and Eiji Warabi for useful comments, Saori Fukui for protein expression, and Erio Ashihara-Fujita for cell culture.

REFERENCES

1. Sutherland, G. R., Baker, E., and Richards, R. I. Fragile sites still breaking. Trends Genet., *14:* 501–506, 1998.
2. Suzuki, H., Komiya, A., Emi, M., Kuramochi, H., Shiraishi, T., Yatani, R., and Shimazaki, J. Three distinct commonly deleted regions of chromosome arm 16q in human primary and metastatic prostate cancers. Genes Chromosomes Cancer, *17:* 225–233, 1996.
3. Driouch, K., Dorion-Bonnet, F., Briffod, M., Champeme, M. H., Longy, M., and Lidereau, R. Loss of heterozygosity on chromosome arm 16q in breast cancer metastases. Genes Chromosomes Cancer, *19:* 185–191, 1997.
4. Chen, T., Sahin, A., and Aldaz, C. M. Deletion map of chromosome 16q in ductal carcinoma *in situ* of the breast: refining a putative tumor suppressor gene region. Cancer Res., *56:* 5605–5609, 1996.
5. Li, C., Berx, G., Larsson, C., Auer, G., Aspenblad, U., Pan, Y., Sundelin, B., Ekman, P., Nordenskjold, M., van Roy, F., and Bergerheim, U. S. Distinct deleted regions on chromosome segment 16q23-24 associated with metastases in prostate cancer. Genes Chromosomes Cancer, *24:* 175–182, 1999.
6. Paige, A. J., Taylor, K. J., Stewart, A., Sgouros, J. G., Gabra, H., Sellar, G. C., Smyth, J. F., Porteous, D. J., and Watson, J. E. A 700-kb physical map of a region of 16q23.2 homozygously deleted in multiple cancers and spanning the common fragile site FRA16D. Cancer Res., *60:* 1690–1697, 2000.
7. Krummel, K. A., Roberts, L. R., Kawakami, M., Glover, T. W., and Smith, D. I. The characterization of the common fragile site FRA16D and its involvement in multiple myeloma translocations. Genomics, *69:* 37–46, 2000.
8. Mashimo, T., Watabe, M., Cuthbert, A. P., Newbold, R. F., Rinker-Schaeffer, C. W., Helfer, E., and Watabe, K. Human chromosome 16 suppresses metastasis but not tumorigenesis in rat prostatic tumor cells. Cancer Res., *58:* 4572–4576, 1998.
9. Bednarek, A. K., Laflin, K. J., Daniel, R. L., Liao, Q., Hawkins, K. A., and Aldaz, C. M. WWOX, a novel WW domain-containing protein mapping to human chromosome 16q23.3-24.1, a region frequently affected in breast cancer. Cancer Res., *60:* 2140–2145, 2000.
10. Ried, K., Finnis, M., Hobson, L., Mangelsdorf, M., Dayan, S., Nancarrow, J. K., Woollatt, E., Kremmidiotis, G., Gardner, A., Venter, D., Baker, E., and Richards, R. I. Common chromosomal fragile site FRA16D sequence: identification of the FOR gene

spanning FRA16D and homozygous deletions and translocation breakpoints in cancer cells. Hum. Mol. Genet., *9:* 1651–1663, 2000.
11. Chang, N. S., Pratt, N., Heath, J., Schultz, L., Sleve, D., Carey, G. B., and Zevotek, N. Hyaluronidase induction of a WW domain-containing oxidoreductase that enhances tumor necrosis factor cytotoxicity. J. Biol. Chem., *276:* 3361–3370, 2001.
12. Paige, A. J., Taylor, K. J., Taylor, C., Hillier, S. G., Farrington, S., Scott, D., Porteous, D. J., Smyth, J. F., Gabra, H., and Watson, J. E. WWOX: a candidate tumor suppressor gene involved in multiple tumor types. Proc. Natl. Acad. Sci. USA, *98:* 11417–11422, 2001.
13. Driouch, K., Prydz, H., Monese, R., Johansen, H., Lidereau, R., and Frengen, E. Alternative transcripts of the candidate tumor suppressor gene, WWOX, are expressed at high levels in human breast tumors. Oncogene, *21:* 1832–1840, 2002.
14. Kuroki, T., Trapasso, F., Shiraishi, T., Alder, H., Mimori, K., Mori, M., and Croce, C. M. Genetic alterations of the tumor suppressor gene WWOX in esophageal squamous cell carcinoma. Cancer Res., *62:* 2258–2260, 2002.
15. Yakicier, M. C., Legoix, P., Vaury, C., Gressin, L., Tubacher, E., Capron, F., Bayer, J., Degott, C., Balabaud, C., and Zucman-Rossi, J. Identification of homozygous deletions at chromosome 16q23 in aflatoxin B1 exposed hepatocellular carcinoma. Oncogene, *20:* 5232–5238, 2001.
16. Yendamuri, S., Kuroki, T., Trapasso, F., Henry, A. C., Dumon, K. R., Huebner, K., Williams, N. N., Kaiser, L. R., and Croce, C. M. WW domain containing oxidoreductase gene expression is altered in non-small cell lung cancer. Cancer Res., *63:* 878–881, 2003.
17. Bednarek, A. K., Keck-Waggoner, C. L., Daniel, R. L., Laflin, K. J., Bergsagel, P. L., Kiguchi, K., Brenner, A. J., and Aldaz, C. M. WWOX, the *FRA16D* gene, behaves as a suppressor of tumor growth. Cancer Res., *61:* 8068–8073, 2001.
18. Yashiro, M., Chung, Y. S., Nishimura, S., Inoue, T., and Sowa, M. Peritoneal metastatic model for human scirrhous gastric carcinoma in nude mice. Clin. Exp. Metastasis, *14:* 43–54, 1996.
19. Fujihara, T., Sawada, T., Hirakawa, K., Chung, Y. S., Yashiro, M., Inoue, T., and Sowa, M. Establishment of lymph node metastatic model for human gastric cancer in nude mice and analysis of factors associated with metastasis. Clin. Exp. Metastasis, *16:* 389–398, 1998.
20. Hippo, Y., Yashiro, M., Ishii, M., Taniguchi, H., Tsutsumi, S., Hirakawa, K., Kodama, T., and Aburatani, H. Differential gene expression profiles of scirrhous gastric cancer cells with high metastatic potential to peritoneum or lymph nodes. Cancer Res., *61:* 889–895, 2001.
21. Ohta, M., Inoue, H., Cotticelli, M. G., Kastury, K., Baffa, R., Palazzo, J., Siprashvili, Z., Mori, M., McCue, P., Druck, T., Croce, C. M., and Huebner, K. The FHIT gene, spanning the chromosome 3p14.2 fragile site and renal carcinoma-associated t(3;8) breakpoint, is abnormal in digestive tract cancers. Cell, *84:* 587–597, 1996.
22. Chang, N. S., Doherty, J., and Ensign, A. JNK1 physically interacts with WW domain-containing oxidoreductase (WOX1) and inhibits WOX1-mediated apoptosis. J. Biol. Chem., *278:* 9195–9202, 2003.

Genome Informatics 14, 34-43 (2003)

Reducing false positives in molecular pattern recognition

Xijin Ge[1] xge@genome.rcast.u-tokyo.ac.jp
Shuichi Tsutsumi[1] shuich@genome.rcast.u-tokyo.ac.jp
Hiroyuki Aburatani[1] haburata-tky@umin.ac.jp
Shuichi Iwata [2] iwata@q.t.u-tokyo.ac.jp

[1] Genome Science Division, Research Center for Advanced Science and Technology, The University of Tokyo, 4-6-1 Komaba, Meguro-ku, Tokyo 153-8904 Japan
[2] Department of Quantum Engineering and Systems Science, School of Engineering, The University of Tokyo, 7-3-1 Hongo, Bunkyo-ku, Tokyo 113-8656 Japan

Abstract

In the search for new cancer subtypes by gene expression profiling, it is essential to avoid misclassifying samples of unknown subtypes as known ones. Therefore, it is necessary to evaluate false positive error rates of various classifiers and to develop robust new algorithms. In this paper, we evaluated several supervised learning algorithms through a 'null-test' by presenting classifiers independent samples that do not belong to any of the tumor types in the training dataset. We found that k-nearest neighbor (KNN) and support vector machine(SVM) could have very high false-positive rates when the number of genes used in prediction is smaller. On the contrary, prototype matching method produce robust predictions when suitable parameters are used. We also introduce a statistical procedure to select optimal gene set for classification. The nonparametric Kruskal-Wallis H test is employed to select genes that are differentially expressed in multiple tumor types. To reduce the redundancy, we divide these genes into clusters with similar expression patterns and select a given number of genes from each cluster. We demonstrate the efficiency of the new algorithm with four publicly available datasets and our own expression database.

Keywords: prototype maching, support vector machine, pattern recognition, cancer diagnosis

1 Introduction

Microarray technology is a promising tool for accurate cancer diagnosis and the searching for new cancer subtypes [1, 2, 3, 4]. Nevertheless, expression data is often very noisy because only a small portion of the genes are correlated with the distinction of tumor subtypes. Even for these genes, variances in expression level can occur for various histological or technical reasons. Additionally, the number of replicates is often limited due to difficulty in collecting human samples. The great challenge is to develop reliable algorithms that fit the needs of current situation.

The first step in such algorithms is to select a set of genes that express differentially in distinct tumor types. In the terms of pattern recognition, this is a task of feature selection that should be distinguished from classification itself. For the binary case concerning two cancer subtypes[1], feature selection can be done by simply looking for those genes that are activated in one patient group while suppressed in the other. In the multiclass problem involving three or more tumor types, feature selection is computationally challenging. The direct approach is to combine multiple pair-wise comparisons with the *all-vs-all* or *one-vs-all* strategy. Due to its simplicity the one-vs-all approach has been employed in several studies[7, 8], in which a given number of genes are selected if they have high expression levels in one tumor type and low expression levels in the others. Selection of genes can also be performed in an iterative manner by observing the performance of a classifier[5].

In this paper we take a different approach for feature selection. Instead of searching the whole list for genes with predefined expression patterns, an unsupervised procedure is proposed to select

all existing patterns of expression that could be useful in classification. This is made possible by introducing clustering analysis techniques, such as K-means clustering, to feature selection.

For the classification of tumors, many machine learning algorithms are available. Besides the simple methods like weighted voting scheme [1] and K nearest neighbor(KNN), support vector machine (SVM) has been widely used by many researchers. Khan *et al.* demonstrated the application of artificial neural networks for discriminating four subtypes of the small, round blue cell tumors (SRBCTs) of childhood[5]. Nevertheless, some comparative studies seem to suggest that simple algorithms tend to have a higher reliability than more complicated ones[11].

In the choice of classification algorithms, we find it important to ask the following questions. If a classifier is trained to discriminate, for example, two subtypes of leukemia, what kind of prediction will it produce for a sample of a newly discovered subtype it has never seen? What if the classifier is presented with normal tissues, or even tissues of stomach cancer? Ideally, these samples should not be classified as either of the two subtypes; otherwise, it would be counted as false positive. Therefore, the above questions lead to the test of false positives. Validation of classifiers in previous studies has been mainly focusing on the false negative cases as most samples for independent tests belong to one of the training subtypes. Despite the importance of avoiding false positives, especially in the process of defining new cancer subtypes and in the detection of metastatic cancers, extensive test of false-positive error rates of various classification schemes have not been reported in the literature.

In this paper, we test the false positive rates of various classification schemes through a 'null-test' in which a classifier is presented with a large number of samples that do not belong to any of the tumor types in the training dataset. To achieve a relatively large dataset, data from 239 microarray experiments performed in several laboratories are pooled together to test the false positive of one classifier. We compare both the false-positive and false-negative error rate of KNN, SVM, and prototype matching (PM), which is perhaps the simplest pattern recognition technique.

2 Method

The whole process of our approach is summarized in Fig. 1A.

2.1 Statistical feature selection

Kruskal-Wallis H test. Kruskal-Wallis H test is the non-parametric counterpart of analysis of variance (ANOVA), which is a standard statistical tool for detecting differences in multi-group comparison. We choose the non-parametric test because it avoids making the assumption that the expression levels are normally distributed with equal variances within groups. It is believed that nonparametric statistical tests are nearly as powerful in detecting differences among populations as parametric methods when the data are normal. They are more powerful in situations where the data does not meet the underlying assumptions of parametric methods. Some statisticians advocate the use of nonparametric methods.

For each gene, a statistic H is calculated according to the ranks of its expression levels between multiple groups. The score is defined as: $H = \frac{12}{N(N+1)} \sum \frac{r_i^2}{n_i} - 3(N+1)$, where N is the number of tumor types in question, r_i is sum of ranks of tumor type i which has n_i samples. The higher H is, the higher the degree of association. The score tells us to what extent the gene expresses differently between *any* two groups. This score is directly related to P values because it follows a χ^2 distribution with $N-1$ degrees of freedom. For $N = 3$ case, if a gene's score is above the critical value of 9.21, we can tell with P<0.01 that this gene correlates significantly with group distinctions. Genes that fail to reach this level of significance are eliminated without further analysis. Note that the statistical significance does not decay with the increase of N. The reason statisticians invent ANOVA and Kruskal-Wallis H test is to avoid the accumulation of errors in multiple pairwise T-test or Mann-Whiteny U test. This

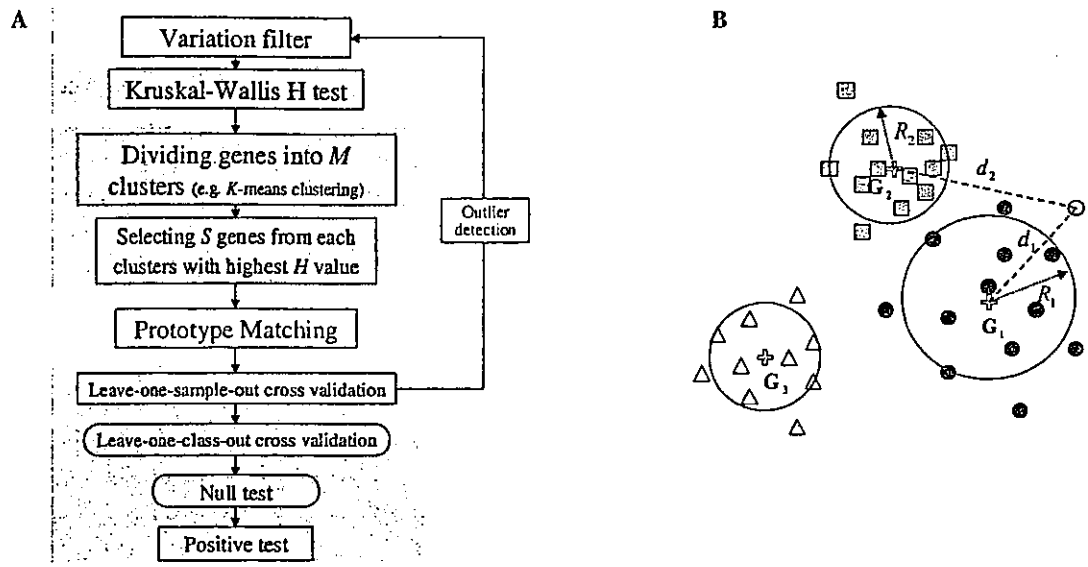

Figure 1: **A,** Outline of cancer classification procedure. Based on non-parametric statistics, a cluster-and-select strategy is employed in the selection of informative genes. False positive errors are tested by null test and leave-one-class-out cross validation (LOCOCV). **B,** Prototype matching. A new sample (open circle) is compared with the existing prototypes.

could happen in *one-vs-all* and *all-vs-all* approaches, where the selection of informative genes is based on $O(N)$ and $O(N^2)$ statistical tests, respectively.

Redundancy reduction: classification of genes for the classification of samples. All those genes that passed the H test convey information that could be useful in classification. But still there are too many of them. We noted that many genes have very similar expression patterns. So it is possible to reduce the size of feature set without incurring classification accuracy. This is the so-called redundancy reduction problem in feature selection[12].

Another issue is that the H score does not tell us which pair-wise distinction a certain gene is associated with. It is possible that there are more genes associated with A-B distinction than those with B-C and C-A, when three subtypes A, B, and C are considered. To improve the overall accuracy of classification, the choice of genes should be made in balance.

We tackle these two problems at the same time through a cluster-and-select strategy. The idea is to select a relatively small number of representatives from each cluster of similarly expressed genes. Methods for clustering analysis have been the subject of extensive research in bioinformatics, and there exist many algorithms. Here we borrowed such techniques for another purpose: gene filtering. We used the simple k-means clustering method, which divides a set of genes into a predefined number of clusters by maximizing the between group variance. In the resultant grouping, some clusters may contain more genes than others. But we select a given number (S) of genes from all clusters to increase the signal-to-noise ratio in classification. Because the H score indicates the significance of association, the genes with higher scores are selected from each group. This is what we call a local filter.

2.2 Prototype matching

Prototype matching is a simple method for pattern recognition. Basically, it stores prototypes and compares a new sample with them. As depicted in Fig. 1B, each tumor type is characterized by an expression prototype G_k and a radius of cluster R_k, where $k = 1, 2, 3$. Prototypes are simply calculated as the average of the expression pattern in training samples, while the radius of each cluster is the average distance between samples and this prototype. Distances are calculated by: $d_{ij} = 1 - P_{ij}$, where

P_{ij} is the Pearson's correlation coefficients between two expression patterns i and j. As $P_{ij} \in [-1, 1]$, we have $d_{ij} \in [0, 2]$.

To demonstrate how PM algorithm works, we use the configuration in Fig. 1B as an example. For a new sample shown in the top right, we calculate its distance to all prototypes and find that d_1, the distance to prototype G_1, is the shortest. Therefore, it is temporarily assigned to type 1. The distance to the second nearest prototype G_2 is also calculated (d_2). The confidence of prediction is measured by the following scores:

$$m = (d_2 - d_1)/d_2, \quad (1)$$

$$d_r = d_1/R_1, \quad (2)$$

$$C = m/d_r. \quad (3)$$

The parameter m characterize the margin of the winner prototype. For an ideal match, where $d_1 \ll d_2$, we have $m \approx 1$. By calculating the parameter d_r, we compare the distance d_1 with the radius of the prototype G_1. Ideally d_r should be about 1.0 or smaller, as R_1 is the average distance. Less typical samples will have a larger d_r. As a larger m and a smaller d_r indicates a confident prediction, we found it is convenient to define a confidence score as $C = m/d_r$. To make confident prediction, we require that the score is larger than a certain threshold (0.08-0.15).

In the example shown in Fig.1B, the new sample is confidently classified as type 1 if C is greater than 0.08. If C fails to reach the threshold value, a 'null' prediction is made. This may be caused by a small m, which indicates that the new sample is almost equally similar to the two best matches. Or, this may also happen if d_r is much larger than 1. In this case, even though the new sample are more similar to the prototype G_1, it deviates from most samples of this kind in the training set so significantly that the difference can no longer be explained in terms of random variance. In addition, the raw Pearson's correlation coefficient between the new sample and prototype G_1 should be larger than 0.2. All together, these criteria help the algorithm avoid false positives. The simplicity of the PM algorithm makes it convenient to impose various common-sense based constraints for making predictions without the significant influence on false negative error rates.

These measures of prediction confidence are chosen empirically. More rigorously, one could assume that the distances to a prototype follow a Gaussian distribution. Thus the mean and standard deviation could be used to evaluate the likeliness that a new sample with distance d_i belongs to a group. Such P values can be calculated for each of the prototypes and the new sample is assigned to the one with the smallest P value. Again, both the absolute P value and the margin should be taken into account to avoid false positives. However, since the number of biological replicates within each cancer type is usually very limited, the mean and standard deviation may not be very reliable. Such approach is not used in the present study. Rather, we used the empirical formulae that are believed to be more robust for small sample size.

For comparison, we also used the closely related KNN and SVM. KNN has many variations in the way that prototypes are chosen from training data and in the ways that votes are weighted[13]. Here a new sample is compared with all the samples in the training dataset. (Unlike PM, KNN uses all the samples in the training dataset as prototypes.) Then the 8-10 nearest neighbors vote with a weight of $1/r$, where r is the rank. The class that receives most votes wins. Confidence is simply characterized by the margin in the percentage of vote. The threshold to make diagnosis prediction is set to as high as 80%, which requires that most of the k neighbors should belong to one class. For SVM, we used an implementation of SVM-FU (www.ai.mit.edu/projects/cbcl) developed by Ryan Rifkin.

2.3 Validation: sensitivity vs. reliability

There are three kinds of predictions errors. A false negative error refers to the case that a null prediction is made for samples that actually belong to the tumor types in the training set. On the contrary, a false positive error corresponds to the case that a positive prediction is made for those

samples that do not belong to any of the tumor types. Also, samples that belong to one of the tumor types may be misclassified. Such cases are usually rare. The performance of classification system should be evaluated with regard to both false negative and false positive.

The false negative error rate is usually evaluated through two tests. In leave-one-sample-out cross validation (LOSOCV), each sample in the training set is withheld and used to test the performance of the classifier trained on the remaining samples. In the 'positive test', independent samples that belong to the training subtypes are presented to a classifier. These samples should be confidently assigned into one of the classes.

To evaluate the false positive error rate, we introduce a 'null test'. In this test, we present a classifier samples that do not belong to any of the categories in the training dataset. Such samples can be, for example, normal tissues or those from other organs. For these samples, a reliable algorithm should produce a 'null' prediction because they should not be assigned to any of the subtypes known to the classifier. Otherwise, a false positive error is registered.

Sometimes, however, null test is impossible due to the lack of samples. An alternative procedure called leave-one-class-out cross validation (LOCOCV) is used. Withholding all the samples that belong to one tumor subtype, we train a classifier with the remaining samples. Then the classifier is tested against false positive error by presenting the samples that are left out. Basically it is a generalization of LOSOCV. The difference is that one withholds a cancer subtype instead of a sample. Note that LOCOCV is only applicable to larger datasets with more subtypes so that the elimination of one cancer subtype does not influence significantly the performance of the classifier. In the next section we apply this procedure to a dataset of 11 cancer types.

2.4 Outliers in the training dataset

The training dataset may contain a small number of outliers due to a variety of reasons such as sample preparation, array experiment, clinical diagnosis, etc. A small number of outliers in the training dataset could seriously degrade the performance of classifiers. As indicated in Fig. 1A, we eliminate such samples from the training dataset according to LOSOCV. We reasoned that the training dataset should be consistent with itself. In our calculation, a sample is considered an outlier if (a) it is misclassified with a high C value when it is not used for training and (b) this single sample exerts un-proportionally large influence on the overall classifier. But one should be very careful with the elimination of samples because the effect of eliminating different samples might be inter-dependent. Additionally, the total number of samples to be eliminated should be kept small (less than 5%). For the detection of outliers, it would be helpful to examine the dataset with some outside programs such as hierarchical clustering and data visualization algorithms.

3 Datasets and Results

Leukemia dataset and the hidden false-positives. The main purpose of the first case of application is to test the efficiency of our statistical feature selection scheme and the robustness of the PM against false positives. For the training dataset, we used the leukemia dataset [1]. This dataset contains expression patterns of samples for acute lymphoblastic leukemia (ALL) and acute myeloid leukemia (AML). As ALL samples can be further divided into two groups: T-cell lineage and B-cell lineage, we consider three subtypes in this dataset. There are 38 samples in the training dataset(11 AML, 19 B-ALL and 8 T-ALL), and 34 independent samples for positive-test. Microarrays used in the experiment are Affymetrix HuFL which contains probes for 6817 human genes. Expression level of a gene is characterized by the average difference score of multiple match and mismatch probe pairs.

To test the false positive rates, we incorporated datasets from several laboratories as the HuFL chip has been widely used and many datasets are available to the public. Our null-test data includes an ovary dataset [6], a dataset of stomach and liver tissue samples, and a variety of other samples from

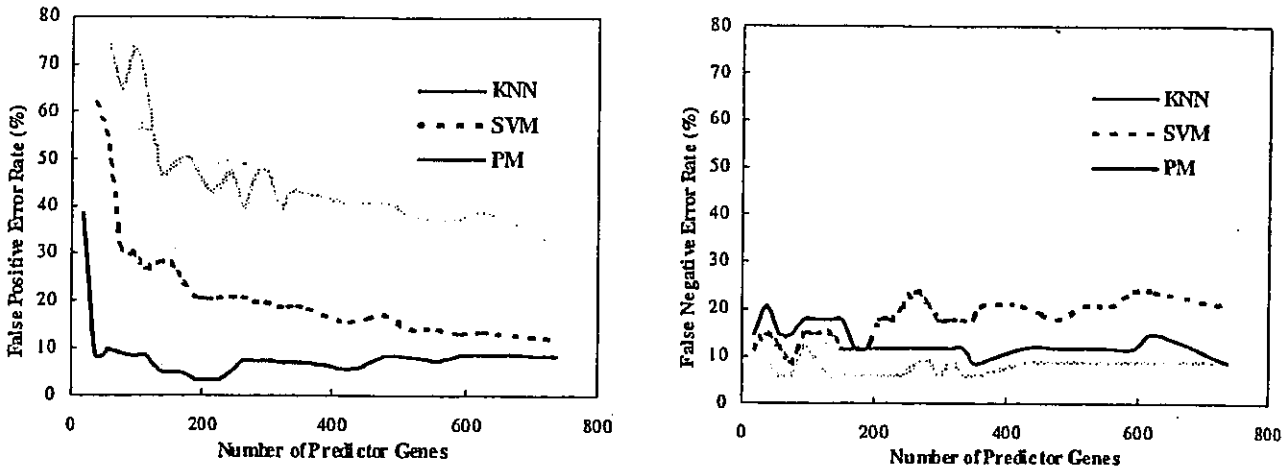

Figure 2: The change of false positive (left) and false negative (right) error rates with the number of genes used for prediction. KNN has the highest false positive error rates and the lowest false negative error rates. For SVM, although we raise the prediction threshold so high that its false negative error rate increases to about 20%, its false positive error rates are still higher than that of PM. This suggests that SVM is intrinsically vulnerable to false positives. The performance of PM are reasonable in both kinds of errors.

our collaborators. These 239 samples are of various origins; they can be any types of human tissues except AML and ALL. See supplementary information for more information about all those samples. Expression scores on each array are normalized to have the same mean and standard deviation to make the data from different laboratories compatible.

In pre-processing, we first eliminate those genes that do not change significantly by requiring that the difference and ratio between the maximum and minimum expression level be larger than 300 and 2, respectively[1]. We also require that the standard deviation and its ratio to mean value be larger than 100 and 0.1. Those genes with a Kruskal-Wallis H score smaller than 9.21 are eliminated as their expression profiles do not correlate with tumor distinction with a statistical significance level P=0.01. The expression levels of the remaining 736 genes are log-transformed. Normalization is done simply by dividing the raw data by the length of a gene's expression vector so that each gene is characterized by a unitary vector. We found that the classification accuracy can be significantly degraded if we follow the popular way of normalization that makes all genes have the same variance.

According to their similarities, these genes are divided into 20 groups by K-means clustering. From each group we selected a small number of genes and construct a feature set. Based on these selected genes, prototype matching is used to make predictions on new samples. The threshold for the prediction confidence C is set to 0.15. By changing the number of genes selected from each cluster, the changes of false negative and false positive error rates are plotted in Fig. 2.

Surprisingly, a large difference is observed in the false positive rates of different classification methods. When less than 100 genes are used, KNN could have a false positive error rate as high as 50%. SVM also has a relatively high error rate of about 20%. On the contrary, PM has an error rate smaller than 10%.

Even with as few as 19 predictor genes, most samples in the positive-test can be correctly classified. This could misleadingly suggest the use of small feature set. But null-test indicates that the false positive rates could be as high as 92% for KNN, 89% for SVM and 38% for PM. Therefore, whatever the classification algorithms, it is important to include several hundreds of genes in the feature set. This shows the importance of null-test: those seemingly irrelevant datasets serve as a background based on which we can tell whether a feature set enables the unique definition of expression prototype for a certain cancer type.

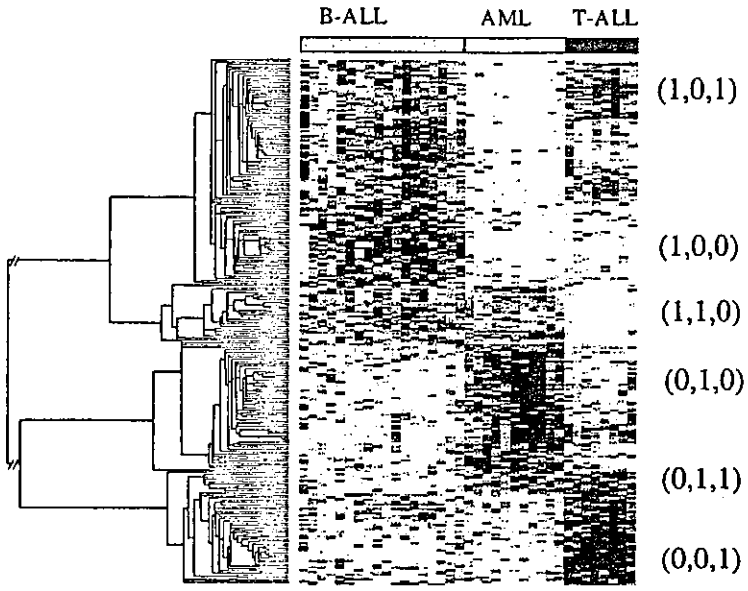

Figure 3: A set of 227 genes chosen for classification of B-cell acute lymphoblastic leukemia (B-ALL), T-cell acute lymphoblastic leukemia (T-ALL), and acute myeloid leukemia (AML)[1]. Instead of searching the whole gene list for predefined expression patterns, we try to find all existing patterns that could be helpful in cancer classification. Black indicates high expression.

From Fig. 2, we also observed that the error rate of PM is not sensitive to the number of genes used in prediction, as long as the number is not too small. Optimizing the balance between two kinds of errors, we finally select 227 genes in our final feature set. In LOSOCV, most of the samples in the training set are correctly classified except 3 false negatives. In the positive and null test, PM has 4 false negatives (11.8%) and 8 false positives(3.3%).

Figure 3 gives these informative genes. The feature set contains all 6 possible alternative expression patterns in a 3-class problem. From top to bottom in the figure, there are genes of type {1,0,1}, {1,0,0}, {1,1,0}, {0,1,0}, {0,1,1}, {0,0,1}, with 1 representing high expression and 0 low expression. Unsurprisingly, at the top region of the figure we find a large number of genes that are shared by B-ALL and T-ALL. We include these genes because we believe they can help achieve a high signal-to-noise ratio. Such genes are ignored in the one-vs-all gene selection method used by [7, 5, 8], as only genes of type {1,0,0}, {0,1,0}, {0,0,1} are selected.

This is further justified by Fig. 1 in supplementary information, in which the false positive error rates using two feature sets are given. With PM, the cluster-and-select method yields more reliable predictions, especially when smaller feature sets are used. This might be attributed to the fact that the new feature selection method includes some very informative genes that are ignored by the conventional method. When more than 500 genes are included in the feature set, error rates tend to be very close. When SVM is applied to these two feature sets, a similar tendency is observed. However, the difference in false positive error rate between feature selection procedures is subtle in comparison with that due to classification algorithms, especially when more genes are used for prediction.

Finally, Fig. 4 shows the distribution of all samples with regard to prediction parameters m and d_r. The x axis is the relative distance to the nearest prototype, while the y axis represents the margin of this prototype over the second nearest one. These two parameters have intuitively simple meanings that could be more easily understood by biologists than parameters like vote percentage or the output of artificial neurons. Because both x and y axes relate to the distances of samples, we refer to such a plot as distance-distance (DD) plot. Most samples in the training and the positive test dataset are located in regions with a large m and small d_r. On the contrary, samples in the null-test dataset have a small m and a large d_r. The decision line for confident prediction $m = td_r$ is also drawn. Here

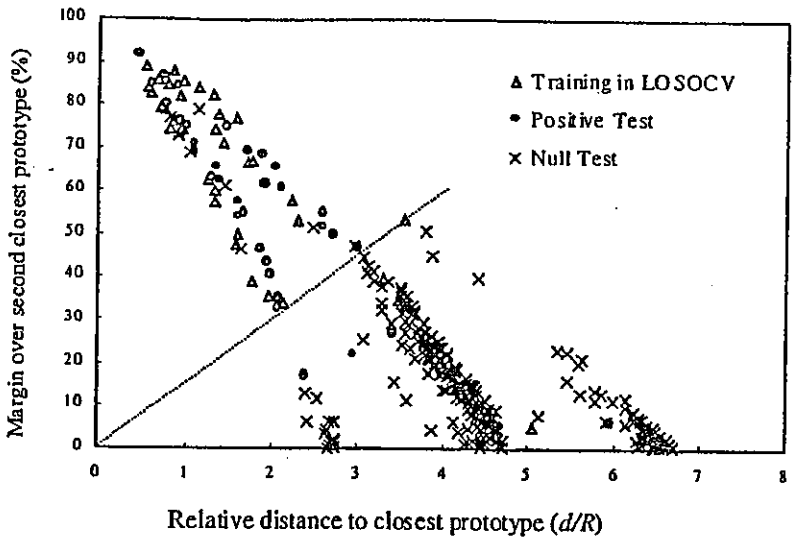

Figure 4: Distribution of samples plotted by two prediction parameters d_r and m. Parameter d_r is the relative distance to the nearest prototype and m is the margin over the second nearest. Positive predictions are made for the samples that lie above the dashed line.

$t = 0.15$ is the slop. In general, the choice of the t can be made according to a plot like Fig. 4, which helps to balance false negative and false positive error.

Extensive testing on other datasets. We then tested the PM algorithm on several other datasets including a lymphoma dataset[4], a SRBCT dataset [5], and the dataset of Su et al.[7]. Prediction results are summarized in table 1. More information is available in the Supplementary Information. The classification scheme proposed in this paper has a relatively lower rate of both false positive and false negative error in these datasets.

Table 1: Summery of four datasets and the performance of PM algorithm. Given in parentheses are the number of misclassified cases observed in leave-one-sample-out-cross-validation (LOSOCV) or independent test. Note that the false negative error rate is calculated according to both LOSOCV and positive test. For the dataset of Su *et al.*, which no independent data for null test is available, a leave-one-class-out-cross-validation (LOCOCV) procedure is employed.

Dataset	# Tumor types	Samples size			False negative	False positive	# Genes used
		Traning	Positive test	Null test			
Leukemia [1]	3	37 (3)	34 (4)	239 (8)	11.8%	3.3%	227
Lymphoma [4]	3	40 (7)	26 (6)	27 (2)	19.7%	7.4%	328
SRBCT [5]	4	63 (6)	20 (2)	6 (0)	9.6%	0%	390
Su *et al.* [7]	11	97 (13)	74 (14)	—(12)	15.8%	12.4%*	400

4 Discussion

There are a wealth of statistical and machine learning tools that could be useful for the classification of cancers. How to pick up the right tools and integrate them is an important issue. Such choice should be made based on knowledge of underlying computational principles. Classification algorithms like SVM and KNN define a hyperplane or hypersurface according to which a multidimensional space of samples are divided into two or more regions (Fig.5). Implicitly, it is assumed that all samples presented to the classifier belong to at least one of the predefined tumor types. This might be true

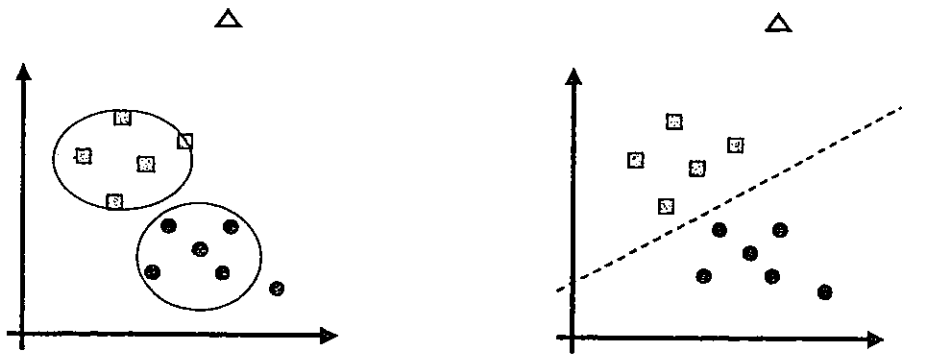

A. Prototype matching (PM)

B. Support vector machine (SVM)

Figure 5: Prototype matching (PM) and support vector machine(SVM) belong to two different paradigms for pattern recognition. While SVM makes prediction for all samples that are far enough from the hyper-plane, PM makes positive predictions only if a new sample is sufficiently similar to a prototype. K-nearest neighbor method is very similar to SVM. As a result, classifiers like PM tend to have more false negatives (e.g. the sample in the bottom right) while those like SVM and KNN may suffer seriously from a high false positive rates(e.g. the sample marked by a triangle at the top).

in some classification tasks such as metastatic vs. non-metastatic tumor[9], or curable vs. incurable DLBCL patients[10]. These are 'true' binary problems, in which SVM and KNN can make accurate predictions. But 'pseudo' binary classification tasks are more freqent: there could exit a third class missing in both training and test dataset. Clinically, the existence of new subtypes of cancers are always possible and it is very difficult to obtain a 'complete' training dataset as required by SVM and KNN. SVM and KNN may have high false positive rates when presented with samples of novel tumor types. This is confirmed in this study (Fig.2).

Unlike SVM and KNN, PM defines a closely bounded region in the multidimensional space to represent each tumor subtypes(Fig.5). There is a large rejection zone that a 'null' prediction will be outputted. The uniqueness of each subtypes is recognized by an expression prototype. Although PM can have a slightly higher false negative rate, false positive error is found to be much lower. Avoiding false positives is essential in the process of discovering new cancer subtypes. Therefore, we believe PM and methods alike might be more suitable for cancer classification.

Our results also give some hints to the question of how many predictive genes should be used in cancer classification. With the inclusion of more genes, we found that false positive errors decrease accordingly. But the opposite tendency is often observed for false negative error. Therefore, the optimal choice should be made by seeking a balance. This could be done by the minimization of the total error rate.

The searching of differentially expressed genes in two or more groups is one of the fundamentally important tasks in the bioinformatics of gene expression analysis. Besides cancer classification, the cluster-and-select feature selection procedure proposed here might be useful in this context. The procedure is able to detect different patterns of gene expression in multiple groups.

To select features from the highly redundant measurements in expression profiling, we employed k-means clustering in addition to a statistics score. Unsupervised classification techniques themselves are used in the process of feature selection for the purpose of supervised classification. This strategy might be useful in other pattern recognition tasks where redundant measurements are involved.

Acknowledgements. We thank Shogo Yamamoto, M. Kano, Jerome Piat, and Naohiro Shichijo for stimulating discussions. We are also greatly indebted to Todd R. Golub for helpful comments on our manuscript and Jiang Fu for proof-reading. Critical comments from the reviews also helped greatly to improve the presentation of this paper.

Supplementary Information. Supplementary information is avalible at web site of Genome Informatics, also available at: www.race.u-tokyo.ac.jp/ xge/cancer/.

References

[1] Golub, T. R. , *et al.*, Molecular classification of cancer: class discovery and class prediction by gene expression monitoring. *Science*, 286:531-537, 1999.

[2] Bhattacharjee A., *et al.*, Classification of human lung carcinomas by mRNA expression profiling reveals distinct adenocarcinoma subclasses.*Proc. Natl. Acad. Sci. USA* 98:13790-13795, 2001.

[3] Ramaswamy,S., & Golub,T. R. DNA microarrays in clinical oncology. *J. CLIN. ONCOL.* 20:1932-1941, 2002.

[4] Alizadeh, A.A.*et al.* The lymphochip: a specialized cDNA microarray for the genomic-scale analysis of gene expression in normal and malignant lymphocytes.*Nature (London)* 403, 503-511, 2000.

[5] Khan, J., *et al.*, Classification and diagnostic prediction of cancers using gene expression profiling and artificial neural networks. *Nature Medicine* 7:673-679, 2001.

[6] Welsh, J. B., *et al.*, Analysis of gene expression profiles in normal and neoplastic ovarian tissue samples identifies candidate molecular markers of epithelial ovarian cancer. *Proc. Natl. Acad. Sci. USA* 98:1176-1181, 2001.

[7] Su, A. I., Welsh, J. B., Sapinoso, L. M., Kern, S. G., Dimitrov, P., Lapp, H., Schultz, P. G., Powell, S. M., Moskaluk, C. A., Frierson, H. F., Jr. & Hampton, G. M. Molecular classification of human carcinomas by use of gene expression signatures. *Cancer Research* 61:7388-7393, 2001.

[8] Ramaswamy S., *et al.*, Multiclass cancer diagnosis using tumor gene expression signatures. *Proc. Natl. Acad. Sci. USA* 98:15149-15154, 2001.

[9] Van 'T Veer L. J., *et al.*, Gene expression profiling predicts clinical outcome of breast cancer. *Nature (London)* 415:530-536, 2002.

[10] Shipp, *et al.*, Diffuse large B-cell lymphoma outcome prediction by gene-expression profiling and supervised machine learning. *Nature Medicine* 8:68-74, 2002.

[11] Dudoit S., Fridlyand J. & Speed T. P. Comparison of discrimination methods for the classification of tumors using gene expression data. *J. Am. Stat. Assoc.* 97:77-87, 2002.

[12] Heydorn, R. P., IEEE Trans. C-2:1051-1054, 1971.

[13] Duda, R. O., Hart, P. E., & Stork, D. G., *Pattern classification* (Wiley, New York, NY), 2001.

[14] Eisen, M. B., Spellman, P. T., Brown, P. O. & Botstein, D. Cluster analysis and display of genome-wide expression patterns. *Proc. Natl. Acad. Sci. USA* 95: 14863-14868, 1998.

[15] Yeang, *et al.*Molecular classification of multiple tumor types. *Bioinformatics* 17 Suppl., S316-S322, 2001.

THE JOURNAL OF BIOLOGICAL CHEMISTRY
Vol. 278, No. 44, Issue of October 31, pp. 43489–43495, 2003
Printed in U.S.A.

Functional Characterization of Rat Brain-specific Organic Anion Transporter (Oatp14) at the Blood-Brain Barrier

HIGH AFFINITY TRANSPORTER FOR THYROXINE*

Received for publication, June 30, 2003
Published, JBC Papers in Press, August 15, 2003, DOI 10.1074/jbc.M306933200

Daisuke Sugiyama‡, Hiroyuki Kusuhara‡, Hirokazu Taniguchi§, Shumpei Ishikawa§, Yoshitane Nozaki‡, Hiroyuki Aburatani§, and Yuichi Sugiyama‡¶

From the ‡Graduate School of Pharmaceutical Sciences, The University of Tokyo, 7-3-1 Hongo, Bunkyo-ku, Tokyo 113-0033, Japan and §Research Center for Advanced Science and Technology, The University of Tokyo, 4-6-1 Komaba, Meguro-ku, Tokyo 153-8904, Japan

Oatp14/blood-brain barrier-specific anion transporter 1 (*Slc21a14*) is a novel member of the organic anion transporting polypeptide (Oatp/OATP) family. Northern blot analysis revealed predominant expression of Oatp14 in the brain, and Western blot analysis revealed its expression in the brain capillary and choroid plexus. Immunohistochemical staining indicated that Oatp14 is expressed in the border of the brain capillary endothelial cells. When expressed in human embryonic kidney 293 cells, Oatp14 transports thyroxine (T_4; prothyroid hormone) (K_m = 0.18 μM), as well as amphipathic organic anions such as 17β estradiol-D-17β-glucuronide (K_m = 10 μM), cerivastatin (K_m = 1.3 μM), and troglitazone sulfate (K_m = 0.76 μM). The uptake of triiodothyronine (T_3), an active form produced from T_4, was significantly greater in Oatp14-expressed cells than in vector-transfected cells, but the transport activity for T_3 was ~6-fold lower that for T_4. The efflux of T_4, preloaded into the cells, from Oatp14-expressed cells was more rapid than that from vector-transfected cells (0.032 *versus* 0.006 min^{-1}). Therefore, Oatp14 can mediate a bidirectional transport of T_4. Sulfobromophthalein, taurocholate, and estrone sulfate were potent inhibitors for Oatp14, whereas digoxin, *p*-aminohippurate, or leukotriene C_4, or organic cations such as tetraetheylammonium or cimetidine had no effect. The expression levels of Oatp14 mRNA and protein were up- and down-regulated under hypo- and hyperthyroid conditions, respectively. Therefore, it may be speculated that Oatp14 plays a role in maintaining the concentration of T_4 and, ultimately, T_3 in the brain by transporting T_4 from the circulating blood to the brain.

Brain capillary endothelial cells are characterized by tightly sealed cellular junctions (tight junctions) and the paucity of fenestra and pinocytotic vesicles, which prevent free exchange between brain and blood (1, 2). Therefore, the uptake of nutrients by the brain occurs through the brain capillary endothelial cells via specific transport systems (3–7). Metabolic enzymes and efflux transporters expressed in the brain capillaries facilitate the elimination of endogenous wastes and xenobiotics from the brain, and restrict their brain accumulation (3–7). Because of these characteristics, the brain capillaries are referred to as the blood-brain barrier (BBB).[1]

The organic anion transporting polypeptides (Oatps in rodents and OATPs in human) belong to the growing gene family of organic anion/prostaglandin transporters that can mediate sodium-independent membrane transport of numerous endogenous and xenobiotic amphipathic compounds (8, 9). Fourteen members of the *Oatp/OATP* gene family have been identified in rodents and humans, and they are classified within the gene superfamily of solute carriers as the *Slc21a/SLC21A* gene family (Human Gene Nomenclature Committee DataBase) (8, 9). Several members of the Oatp/OATP family have been identified in the brain (Oatp1–3 and moat1 in rodents and OATP-A in human) (10–14). Especially, in the BBB, rat Oatp2 and human OATP-A have been shown to be expressed in the plasma membrane of the brain capillary endothelial cells (15, 16). Involvement of rat Oatp2 in the uptake and efflux transport of its substrates was investigated *in vivo* (17, 18). The uptake of [D-penicillamine^{2,5}]-enkephalin (DPDPE) from the blood to the brain was determined by the brain perfusion technique in the presence and absence of Oatp2 inhibitors (17). The brain uptake of DPDPE was increased in Mdr1a (P-glycoprotein) gene knockout mice, and the uptake in Mdr1a knockout mice was inhibited by the substrates and inhibitors of rat Oatp2 such as digoxin and 17β estradiol-D-17β-glucuronide ($E_2$17βG). Vice versa, when $E_2$17βG was microinjected into the cerebral cortex, the subsequent elimination of $E_2$17βG from the brain was carrier-mediated (18), and the elimination of $E_2$17βG was completely inhibited by co-administration of taurocholate and probenecid, whereas digoxin had only a partial effect (18). Partial inhibition by digoxin suggested that additional efflux transport system(s) for $E_2$17βG, which is taurocholate- and probenecid-sensitive, is involved in the brain capillary.

Li *et al.* (19) recently identified BBB-specific anion trans-

* This work was supported by grants-in-aid from the Ministry of Health, Labor and Welfare of Japan. The costs of publication of this article were defrayed in part by the payment of page charges. This article must therefore be hereby marked "*advertisement*" in accordance with 18 U.S.C. Section 1734 solely to indicate this fact.

¶ To whom correspondence should be addressed: Dept. of Molecular Pharmacokinetics, Graduate School of Pharmaceutical Sciences, The University of Tokyo, 7-3-1 Hongo, Bunkyo-ku, Tokyo 113-0033, Japan. Tel.: 81-3-5841-4770; Fax: 81-3-5841-4766; E-mail: sugiyama@mol.f.u-tokyo.ac.jp.

[1] The abbreviations used are: BBB, blood-brain barrier; Oatp, organic anion transporting polypeptide; BSAT, BBB-specific anion transporter; HEK293, human embryonic kidney 293; CA, cholate; GCA, glycocholate; LCA, lithocholate; CDCA, chenodeoxycholate; UDCA, ursodeoxycholate; PGD_2, prostaglandin D_2; PGE_2, prostaglandin E_2; E3040, 6-hydroxy-5,7-dimethyl-2-methylamino-4-(3-pyridylmethyl) benzothiazole; PBS, phosphate-buffered saline; DPDPE, [D-penicillamine^{2,5}]-enkephalin; $E_2$17βG, 17β estradiol-D-17β-glucuronide; T_4, thyroxine; TLCS, taurolithocholate sulfate; 4-MUS, 4-methylumbelliferone sulfate; TRO-S, troglitazone sulfate; RT, reverse transcriptase; MMI, methimazole; T_3, triiodothyronine; ES, estrone sulfate; BSP, sulfobromophthalein; LT, leukotriene; D2, type 2 iodothyronine deiodinase.